Accepted Manuscript

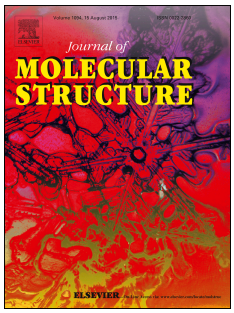

Conformational, vibrational and DFT studies of a newly synthesized arylpiperazine-based drug and evaluation of its reactivity towards the human GABA receptor

A.T. Onawole, A.F. Al-Ahmadi, Y.S. Mary, C.Y. Panicker, N. Ullah, S. Armaković, S.J. Armaković, C.V. Alsenoy, A.A. Al-Saadi

PII: S0022-2860(17)30888-8

DOI: 10.1016/j.molstruc.2017.06.107

Reference: MOLSTR 23993

To appear in: *Journal of Molecular Structure*

Received Date: 20 May 2017

Revised Date: 21 June 2017

Accepted Date: 21 June 2017

Please cite this article as: A.T. Onawole, A.F. Al-Ahmadi, Y.S. Mary, C.Y. Panicker, N. Ullah, S. Armaković, S.J. Armaković, C.V. Alsenoy, A.A. Al-Saadi, Conformational, vibrational and DFT studies of a newly synthesized arylpiperazine-based drug and evaluation of its reactivity towards the human GABA receptor, *Journal of Molecular Structure* (2017), doi: 10.1016/j.molstruc.2017.06.107.

Conformational, vibrational and DFT studies of a newly synthesized arylpiperazine-based drug and evaluation of its reactivity towards the human GABA receptor

A. T. Onawole[a], A. F. Al-Ahmadi[a], Y.S. Mary[b], C.Y. Panicker[b], N. Ullah[a], S. Armaković[c], S. J. Armaković[d], C.V. Alsenoy[e], A. A. Al-Saadi[a,*]

[a] Department of Chemistry, King Fahd University of Petroleum and Minerals, Dhahran 31261, Saudi Arabia
[b] Department of Physics, Fatima Mata National College, Kollam, Kerala, India
[c] University of Novi Sad, Faculty of Sciences, Department of Physics, Trg D. Obradovića 4, 21000 Novi Sad, Serbia
[d] University of Novi Sad, Faculty of Sciences, Department of Chemistry, Biochemistry and Environmental Protection, Trg D. Obradovića 3, 21000 Novi Sad, Serbia
[e] Department of Chemistry, University of Antwerp, Groenenborgerlaan 171, B-2020, Antwerp, Belgium
[*] Corresponding Author: asaadi@kfupm.edu.sa

Abstract

This study reports a computational assessment of important biochemical properties and vibrational assignments for the synthesized 1-(4-(3-methoxy-4-nitrophenyl)piperazin-1-yl)ethanone (MNPE). MNPE is related to the commonly used arylpiperazine-based drugs that exhibit a wide range of pharmacological activities. The characterization of MNPE is based on the readily sighted 1363 cm^{-1} infrared band (associated with piperazine ring stretching), 1308 cm^{-1} Raman line (associated with the phenyl ring breathing), 1242 cm^{-1} Raman line and 1092 cm^{-1} infrared band (both associated with C-N stretching) as key modes in its vibrational spectra. First principle calculations revealed that MNPE could exist in sixteen different plausible conformations, which were used as basis to understand the possible molecular docking mechanism of the molecule as an agonist in the human $GABA_A$ receptor. The best binding scenarios showed the presence of intramolecular hydrogen bonding in MNPE and was comparable with the most stable configuration. It was further evaluated for its reactivity properties by utilizing the concepts of Average Local Ionization Energies (ALIE) and Fukui functions. The autoxidation and hydrolysis degradation likelihood of MNPE estimated from the computed bond dissociation energies and radial distribution functions predicted that MNPE is to be readily biodegradable in aqueous solutions.

Keywords: Arylpiperazine; Human $GABA_A$ receptor; Molecular docking; Vibrational spectroscopy; Density functional theory.

1. Introduction

Arylpiperazines and its derivatives have demonstrated an alluring pharmacological framework that is found in different branded drugs. The inclusion of piperazine motif is a vital synthetic procedure in drug discovery. This is due to its solubility, proper alkalinity, and hydrogen bond formation capability. All these attributes in turn lead to its ease in the modification of molecular physicochemical properties [1, 2]. Moreover, arylpiperazine derivatives have found extensive applications in the pharmaceutical chemistry such as anticancer [3, 4], antiviral [5], antifungal [6], anti-oxidative [7], anti-histamine [8], anti-parasitic [9] psychotolytic [10] and as an agonist for the human GABA receptor [11]. Contrary, the frequent usage and improper disposal of this class of compounds can act as organic pollutants and pose threat to the environment especially in water and hence become toxic to aquatic organisms [12-14]. In general, arylpiperazine derivatives are quite stable and hence their degradation under normal conditions is very slow. This in turn make the conventional water purification methods unsuitable for efficient and economic removal of these compounds [15]. Therefore, considerable synthetic efforts have been devoted to design new arylpiperazines which are both medicinally effective and water-degradable. In the light of above, we have synthesized an arylpiperazine derivative and have studied it computationally and spectroscopically as well as by means of bond dissociation energy (BDE), radial distribution function (RDF) and molecular docking approaches to gain some insights on its electronic properties and side effects.

Given the fact that the advanced oxidation is considered a widely used method in water purification technology [16], understanding the reactive properties of MNPE (Fig. 1) and the possible auto-oxidation locations within the molecule is essential. This in turn can be achieved by calculating BDEs during hydrogen abstraction. Thus, the BDE of the rest of the single acyclic bonds can be used for classification of bonds according to their strength and prediction of locations where degradation can occur. Considering the importance of water as solvent, molecular dynamics (MD) simulations can provide valuable information to ascertain the interaction with water molecules and different type of atoms of MNPE. In this case, RDF shall be particularly quite useful.

In addition, arylpiperazine derivatives are known as agonist to naturally occurring γ-aminobutyric acid (GABA) receptor, which in turn produces a synergistic anti-stress and anti-

anxiety effect. The $GABA_A$ receptor is one of the Ligand-gated Ion Channels (LICs) that are referred to as ionotropic receptors because they allow the passage of ions such as Na^+ and K^+ through the membrane as a response to the stimulus effect when a ligand binds to them. [17–19]. Since most drugs often imitate the action of endogenous ligands [20a], the conformational analysis and the molecular docking study of can thus provide a deeper understanding of the mode of action by which drugs act on such a target protein.

2. Experimental

Melting Points were determined on a Büchi apparatus (Büchi Labortechnik AG, Switzerland) and are uncorrected. Elemental analysis was carried out on a Perkin Elmer Elemental Analyzer Series 11 Model 2400 (PerkinElmer Inc. USA). ^1H and ^{13}C NMR spectra were measured in $CDCl_3$ using TMS as internal standard on a JEOL JNM-LA 500 MHz spectrometer (JEOL USA Inc.). Analytical TLC was carried out on silica gel 60 F_{254} plates (E. Merck); column chromatography was carried out on silica gel (200-400 mesh, E. Merck). DR/Jasco FT-IR 6300 spectrometer employing KBr tablets was used to record the infrared spectrum (Fig. 2) of MNPE while a Bruker RFS 100/s, Germany was used to record the Raman spectrum (Fig. 3). The emission of Nd:YAG laser at the wavelength of 1064 nm was utilized for sample excitation with a maximal power of 150 mW.

2.1 Synthesis of MNPE (**6**)

To a suspension of compound **5** [20b] (1.05 g, 3 mmol) in CH_2Cl_2 (20 mL) at 0 ^oC was added Et_3N (1.1 mL, 8 mmol) followed by the dropwise addition of acetyl chloride (0.32 mL, 4.5 mmol). The mixture was stirred for three hours at room temperature until completion (TLC analysis). The reaction was quenched with saturated $NaHCO_3$ (10 mL) and the organic layer was separated, washed with H_2O (10 mL) and then dried over Na_2SO_4 followed by evaporation under reduced pressure to obtain a yellow solid, which was re-crystallized with ethanol to afford the title compound **6** as yellow crystalline solid. ^1H NMR (500 MHz, $CDCl_3$): δ 2.16 (s, 3H, $COCH_3$), 3.41 (m, 4H, piperazine H), 3.68 (2H, t, piperazine H), 3.80 (2H, t, piperazine H), 3.91 (s, 3H, OCH_3), 6.35 (d, J = 1.9 Hz, 1H, H-2), 6.41 (dd, J = 1.9, 8.6 Hz, 1H, H-6), 8.01 (d, J = 8.6 Hz, 1H, H-5). Anal. Calcd for $C_{13}H_{17}N_3O_4$: C, 55.91; H, 6.14; N, 15.05%. Found: C, 55.87; H, 6.17; N, 15.01.

3. Computational Details

An extensive conformational analysis was done for MNPE using Density Functional Theory (DFT) with Gaussian 09 program [21] at the Becke's three-parameter half-and-half model and the Lee-Yang-Parr connection useful (B3LYP) level of theory using both 6-311G(d,p) and 6-311++G(d,p) as the basis sets which are good for medium-size organic molecules. Sixteen possible structures (Fig. 4) of MNPE were determined, and their energies were computed (Table 1) [22]. The 6-311++G(d,p) basis set was employed to predict the geometrical parameters in details (Tables 2-5) and calculate the vibrational wavenumbers (Table 5) [23], [24] of the most stable conformer (Fig. 1) using a scaling factor of 0.9613 [25]in order to acheive a better correlation with experimental values. The assignments of the figured wavenumbers are supported by the atomic displacements visulized with GAUSSVIEW [26] and the Potential Energy Distribution (PED) values computed with the GAR2PED software [27].

Moreover, the Jaguar program 9.0 embedded in the Schrödinger Materials Science Suite [28] was utilized for DFT calculations of Average Local Ionization Energies (ALIE), Fukui capacities and BDE. For MD simulations of RDFs, the Desmond program [29]–[32] was utilized, likewise as executed in the Schrödinger Materials Science Suite. For all DFT estimations B3LYP exchange correlation functionals were employed [33]. . Concerning MD simulations, OPLS 2005 force field [34] was used. The system was modeled by placing one molecule of MNPE in a cubic box with ~3000 water molecules and treated with NPT (where N is constant particle number, P is pressure and T is temperature) ensemble class. The Pressure was set to 1.0325 bar while the temperature was set to be 300 K, with simulation time of 10 ns. The cut-off radius was set to 12 Å, while the solvent description was done by employing the Simple Point Charge (SPC) model [35]. The molecular docking analysis was performed with the CLC Drug Discovery program [36] while the Moleman 2 [37] was used to validate the crystal structure of the human $GABA_A$ receptor which is the target protein in this study.

4 Results and Discussion

4.1 Synthesis of 1-(4-(3-methoxy-4-nitrophenyl)piperazin-1-yl)ethanone

The desired compound MNPE (**6**) was synthesized as outlined in scheme 1. In brief, O-methylation of phenol 1 with iodomethane in DMF rendered **2**, which in turn was condensed

with 1-boc-piperazine **3** to produce coupled product **4**. Acid induced removal of boc protection of **4** furnished salt **5**, which was reacted with acetic anhydride in CH_2Cl_2 to yield the desired **6** in 44% overall yield from **1** [38].

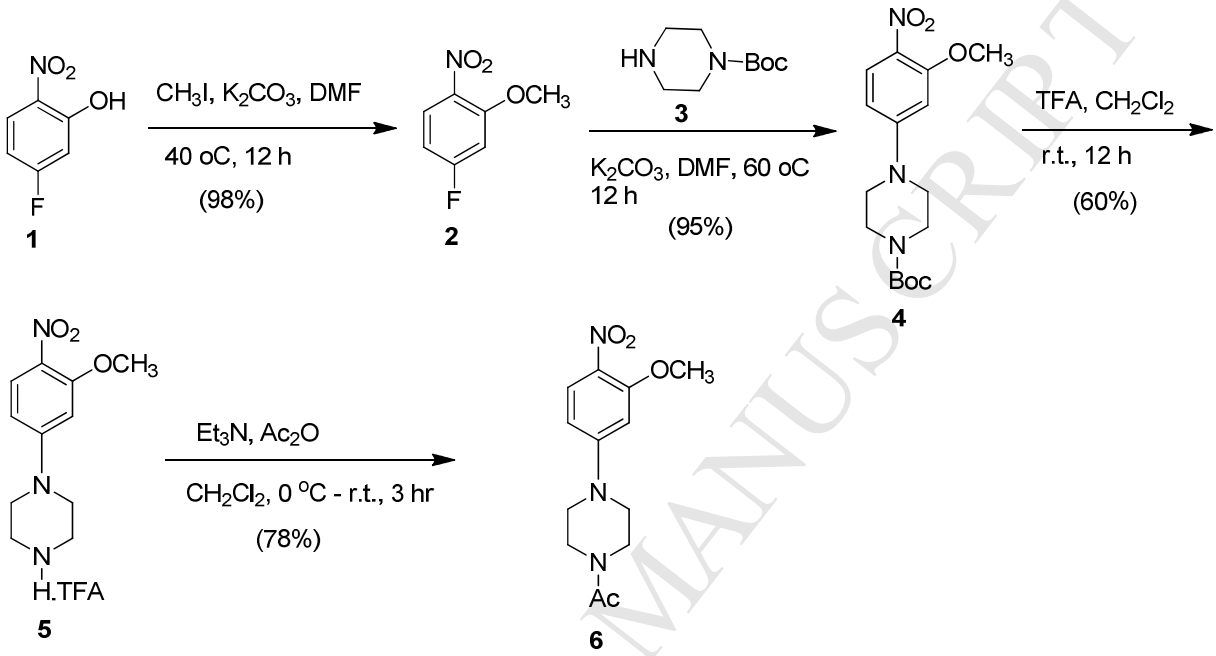

Scheme 1. Synthesis of 1-(4-(3-methoxy-4-nitrophenyl)piperazin-1-yl)ethanone (MNPE)

4.2. Conformational Analysis

Exploring conformational properties of organic-based drugs is extremely useful in order to understand the structure-activity relationship. Detailed conformational analysis of the multi-rotor MNPE has led to 16 possible unique conformations depicted in Fig. 4. The variation of bond lengths, bond angles and dihedral angles among the stable forms are listed in Tables 2-4. Generally, the steric effect when the methoxy and nitro groups repel each other pushes the energy 1-2 kcal/mol to the higher side (Table 1). Consequently, the position of the methoxy with respect to the nitro groups is the main factor that influences the overall energy of the molecule. The average distance between O_{13} and O_{37} in A and B conformations is about 0.2 Å shorter than in corresponding C and D conformations (Table 2). The internal rotation of the OCH_3 group,

presented in Fig. 5(A), has shown that the eclipsing position of the CH_3 group is 3-4 kcal higher in energy than when the methoxy and nitro group oxygens repel each other. On the other hand, the molecule seems more flexible flipping along the aromatic ring-piperazine ring linkage and the nitro group-aromatic ring linkage. The piperazine ring in its lowest energy form positons itself in the same plane of the benzene ring with about 42º tilting angle. The stable position of the methoxy group in C and D configurations represents a metastable arrangement with 5 kcal/mol barrier (Fig. 5) to interchange to A and B conformations.

The conformer B4 is predicted to be the most stable form, and its detailed structural parameters are listed in Table S1. There is no significant difference between the results obtained by the B3LYP/6-311G(d,p) and B3LYP/6-311++G(d,p) basis sets in terms of bond angles and distances, yet some major dihedral angles, such as O_{37}-N_{15}-C_{10}-C_9 and O_{36}-N_{15}-C_{10}-C_{11} (Table 4) showed a notable difference (up to 6º in some cases) when these two different basis sets are utilized. This perception demonstrates the impact of the electronic properties of the nitro group when long-range repulsion parameters are considered in the basis set.

The molecular electrostatic potential (MEP) map (Fig 6a) indicates that the nitro and carbonyl groups demonstrate an electronegative region in the molecule whereas the electropositive region occurs at the piperazine ring vicinity. This map has given an insight into possible interactions between MNPE and the amino acid in the target protein. The HOMO (highest occupied molecular orbital) and LUMO (lowest unoccupied molecular orbital) energy values were calculated to be -7.83 eV and -4.55 eV, respectively, with an energy gap of 3.28 eV. Due to the relatively small gap in MNPE, the charge transfer process is predicted to be feasible and supports the docked pose of the compound in the molecular docking analysis, which will be discussed later in this script.

4.3 Geometrical Parameters for B4 Conformer

For the piperazine ring of the title compound, the bond lengths are computed as N_4-C_5 = 1.4586 Å, N_4-C_3 = 1.4567 Å, C_3-C_2 = 1.5293 Å, N_1-C_6 = 1.4633 Å, N_1-C_2 = 1.4675 Å, C_5-C_6 = 1.5284 Å and corresponding reported bond lengths are 1.465, 1.463, 1.514, 1.458, 1.471, 1.511Å [39] and 1.4488, 1.485, 1.535, 1.488, 1.477, 1.547 Å [40]. The DFT calculations predict the bond angles within the piperazine ring N_4-C_3-C_2 = 110.4°, N_4-C_5-C_6 = 111.1°, N_1-C_6-C_5 = 110.9°, N_1-C_2-C_3 = 111.3°, C_6-N_1-C_2 = 112.4° whereas the corresponding reported values are 110.4, 113.1,

110.7, 109.7, 114.8° [40] and 110.0, 109.7, 109.7, 110.0, 110.0° [39].The dihedral angles of the piperazine ring, C_5-N_4-C_3-C_2 = -54.7°, C_6-N_1-C_2-C_3 = -55.1°, N_4-C_3-C_2-N_1= 53.9°, C_2-N_1-C_6-C_5 = 54.6°, C_3-N_4-C_5-C_6 = 54.9°, N_1-C_6-C_5-N_4 = -53.6° are in agreement with the reported values [41]. The C-O bond lengths of MNPE are C_9-O_{13} = 1.346 Å and C_{14}-O_{13} = 1.424 Å and the increase in bond length of C_{14}-O_{13} is due to the noticeable hydrogen bonding experienced by the molecule as reported in literature [42], [43]. In the present case, the C=O bond length is 1.2225 Å which is in agreement with literature [44]. The C-C bond lengths in the phenyl ring are in the range 1.3792-1.4118 Å and the bond lengths are somewhere in between the normal values for a single (1.54 Å) and a double (1.33 Å) bond [44]. For the title compound the N-O bond lengths are 1.2246 Å and 1.2324 Å which was in agreement with reported values [45].

The C-N-O angles are reported as 117.7° and 117.5° [45] where as for the title compound, the angles are 118.9° and 117.0°. At N_{15} position, the bond angles are, C_{10}-N_{15}-O_{37} = 118.9°, C_{10}-N_{15}-O_{36}= 117.0° and O_{36}-N_{15}-O_{37} = 124.1° and this asymmetry in angles is due to the adjacent OCH_3 group. At C_{10} position, the bond angle C_9-C_{10}-C_{15} increased by 2.9° and C_{11}-C_{10}-N_{15} is decreased by 2.5° from 120°, which reveals the hydrogen bonding with the H_{31} atom. At C_9 position, the bond angles are, C_8-C_9-C_{10} = 118.5°, C_8-C_9-O_{13} = 122.9° and C_{10}-C_9-O_{13} = 118.5° and the increase in C_8-C_9-O_{13} is due to the interaction between CH_3 and H_{30} atom. At C_7 position the bond angles are C_8-C_7-C_{12} = 118.0°, C_8-C_7-N_1 = 121.4° and C_{12}-C_7-N_1 = 120.5° and the asymmetry in angles is due to the interaction between the phenyl ring and the CH_2 groups of piperazine ring. Similarly, at C_{16} position, the bond angles are, N_4-C_{16}-C_{18} = 117.5°, N_4-C_{16}-O_{17} = 121.5°, C_{18}-C_{16}-O_{17} = 121.0° and this asymmetry is due to the CH_3 group and CH_2 groups of piperazine ring. The methoxy group is slightly tilted from the phenyl ring as is evident from the torsion angles, C_7-C_8-C_9-O_{13} = 177.6°, C_8-C_9-O_{13}-C_{14} = 1.9°, C_{11}-C_{10}-C_9-O_{13} = -175.9° and C_{10}-C_9-O_{13}-C_{14} = 178.8° and the phenyl ring and piperazine ring are tilted from each other as is evident from the torsion angles, C_8-C_7-N_1-C_6 = -4.7°, C_8-C_7-N_1-C_2 = 139.3°, C_{12}-C_7-N_1-C_2 = -42.2° and C_{12}-C_7-N_1-C_6 = 173.7°. The $COCH_3$ and the piperazine ring are tilted from each other as is evident from the torsion angles, C_5-N_4-C_{16}-O_{17} = 4.1°, C_3-N_4-C_{16}-O_{17} = 174.7°, C_5-N_4-C_{16}-C_{18} = -176.4° and C_3-N_4-C_{16}-C_{18} = -5.8°.

4.4 Molecular Reactivity

4.4.1 ALIE Surfaces and Fukui Functions

Two representative Average Local Ionization Energy (ALIE) surfaces of MNPE are depicted in Fig. 7a. ALIE is frequently used as a quantum molecular descriptor for the understanding of local reactivity properties of molecular systems. This quantity was introduced by Sjoberg *et al.* [46, 47], and it is useful when its values are mapped to the electron density surface. In that case the certain areas of the surface indicate the molecule locations where electrons are the least tightly bound, i.e. the most easily removed. Therefore these locations are the most prone to electrophilic attacks. ALIE is defined as followed:

$$I(r) = \sum_i \frac{\rho_i(\vec{r})|\varepsilon_i|}{\rho(\vec{r})} \tag{1}$$

where $\rho_i(\vec{r})$ represents the electronic density of the *i*-th molecular orbital at the point $\vec{r}$, ε_i represents the orbital energy and $\rho(\vec{r})$ is the total electronic density function.

The results obtained for MNPE revealed that the locations at the benzene ring and NO_2 group are prone to possible electrophilic attack. This implied that electrons in the regions near vicinity of carbon atoms C_8 and C_{12} (belonging to benzene ring), nitrogen atom N_1 (belonging to piperazine ring) and oxygen atoms of NO_2 group are less tightly bound. At all these locations, the ALIE values were somewhat lower than 200 kcal/mol, exhibiting possible reactive sites.

Besides MEP and ALIE analysis, values of Fukui functions (Fig. 7b) can also serve as indicators of possible reactive centers in the molecule. They provide insight on how electron density changes with the addition or removal of the charge. Two Fukui functions, f^+ and f^-, were calculated with infinite difference approach as follows:

$$f^+ = \frac{\left(\rho^{N+\delta}(r) - \rho^N(r)\right)}{\delta} \tag{2}$$

$$f^- = \frac{\left(\rho^{N-\delta}(r) - \rho^N(r)\right)}{\delta} \tag{3}$$

where *N* is the number of electrons in the reference state of the molecule and δ represents the fraction of electron, which is set to be 0.01 [48].

According to the results presented in Fig.6a, purple region of Fukui f^+ function is located at oxygen atoms of NO_2 group, which indicated an increase in the electron density with the addition of charge. On the other side, the negative color was generated at the methyl group in the near vicinity of benzene ring and in the near vicinity of oxygen atom O_{13}, which revealed these

locations as interesting possible reactive centers. It is evident that the regions indicated by Fukui functions corresponded to the regions where MEP surfaces have the highest or lowest values.

4.4.2 NBO Analysis

The natural bond orbitals (NBO) calculations were performed using NBO 3.1 program [49] as implemented in the Gaussian 09 [21] package, and various hyper-conjugative interaction parameters are given in tables 7 and 8. The intra-molecular hyper-conjugative interactions in the title compound are: C_7-C_8 from N_1 of $n_1(N_1)\rightarrow\pi^*(C_7\text{-}C_8)$, C_{16}-O_{17} from N_4 of $n_1(N_4)\rightarrow\pi^*(C_{16}\text{-}O_{17})$, C_9-C_{10} from O_{13} of $n_2(O_{13})\rightarrow\pi^*(C_9\text{-}C_{10})$, N_4-C_{16} from O_{17} of $n_2(O_{17})\rightarrow\sigma^*(N_4\text{-}C_{16})$, N_{15}-O_{37} from O_{36} of $n_3(O_{36})\rightarrow\pi^*(N_{15}\text{-}O_{37})$, N_{15}-O_{36} from O_{37} of $n_2(O_{37})\rightarrow\sigma^*(N_{15}\text{-}O_{36})$ having electron densities, 0.42457, 0.28120, 0.46950, 0.08444, 0.62299, 0.06304e and stabilization energies, 32.39, 62.42, 35.28, 26.34, 148.77, 19.69 KJ/mol.

From Table 7, the natural hybrid orbital with higher energies, considerable p-character (nearly 100%) and low occupancy were predicted to be $n_2(O_{13})$, $n_2(O_{17})$, $n_3(O_{36})$ and $n_2(O_{37})$ with energies, -0.31933, -0.24010, -0.25443, -0.26721a.u and p-characters, 99.99, 99.99, 99.84, 99.97% and occupation numbers, 1.81466, 1.86423, 1.46681, 1.89783, respectively. On the other hand, the orbitals with lower energies and high occupancy are: $n_1(O_{13})$, $n_1(O_{17})$, $n_1(O_{36})$, $n_1(O_{37})$ with energies, -0.54441, -0.77681, -0.66876, -0.77363a.u and p-characters, 62.67, 41.68, 24.97, 25.40% and occupation numbers, 1.96232, 1.97565, 1.98127, 1.98091, respectively.

Thus, a nearly pure p-type lone pair orbital is predicted to participate in the electron donation to the $n_1(N_1) \rightarrow \pi^*(C_7\text{-}C_8)$, $n_1(N_4) \rightarrow \pi^*(C_{16}\text{-}O_{17})$, $n_2(O_{13}) \rightarrow \pi^*(C_9\text{-}C_{10})$, $n_2(O_{17}) \rightarrow \sigma^*(N_4\text{-}C_{16})$, $n_3(O_{36}) \rightarrow \pi^*(N_{15}\text{-}O_{37})$, and $n_2(O_{37}) \rightarrow \sigma^*(N_{15}\text{-}O_{36})$ interactions in MNPE.

4.5 Degradation Properties

The degradation properties based on the autoxidation and hydrolysis processes of MNPE can be perceived with the help of computed Bond Dissociation Energy (BDE) values as obtained by DFT calculations [50, 53]. BDE is a valuable tool for primary assessment of molecular sites wherein the mechanism of autoxidation could initiate. In addition, the efficiency of autoxidation process is related to the abstraction of hydrogen atom by peroxy radical from the parent drug molecule [50, 51]. It is well established that all peroxy radicals have similar BDE values (in the

range of 87 kcal/mol to 92 kcal/mol). When the calculated BDE for hydrogen abstraction is within this range, corresponding molecule location is considered a candidate for the initiation of the autoxidation process. BDE values for peroxy radicals can be considered independent of the chemical surrounding [51, 52]. When the BDE value of the hydrogen abstraction is in the interval of 75 kcal/mol to 85 kcal/mol, then the molecule is considered to be highly prone to autoxidation mechanism [50], [53]. BDE values of all single acyclic bonds of the title molecule are presented in Fig. 8. All BDE values related to hydrogen abstraction are higher than 92 kcal/mol, thus it indicates that MNPE is highly stable in open air, in the presence of oxygen. On the other hand, two BDE values for the rest of the single acyclic bonds were predicted to have values of ~66 and ~69 kcal/mol, indicating that acetyl-phenyl linkage and O-CH_3 bond are dissociable and hence can be a potential site of degradation.

Furthermore, molecular areas that are likely to interact with water molecules are presented in Fig. 9 in the form of Radial Distribution Functions (RDFs), which was obtained from MD simulations. RDF, $g(r)$, is the probability of finding a particle in the distance r from another particle [54]. When the obtained curve profile is sharp and when its peak is at a short distance, it indicates interactions between certain atoms and water molecules.

RDF curves shown in Fig. 9a indicate that the carbon atoms C_{10}, C_{14} and C_{18} could have pronounced interactions with water molecules. Atoms C_{10} and C_{18} are very similar in terms of the highest $g(r)$ value, ranging between 1.3 and 1.5, and its peak distance, which has a value of around 3.6 Å. On the other side carbon atom C_{14} shows the highest $g(r)$ value of 1.1 and a peak distance at around 4.7 Å. Moreover, RDFs of non-carbon atoms demonstrate that they are more apt to interact with water molecules (Fig. 9b). The shortest peak distances in these cases were calculated to be for N_1 and O_{17} atoms, both less than 3 Å, with maximal $g(r)$ values of around 0.5 and 1.0, respectively. O_{36} and O_{37} are very similar in terms of $g(r)$ value and peak distance, around 1.1 and 3.2 Å, respectively. Nitrogen atom N_{15} has scored the highest $g(r)$ value of almost 1.4, while its peak distance is located at somewhat less than 4 Å. Nitrogen atom N_4 has maximal $g(r)$ value of around 1.2 with its peak distance located at around 4.7 Å. The facts that BDE values are the lowest for bonds that connect nitro and methoxy moieties to the benzene ring and that RDF curves show pronounced interactions for certain atoms belonging to these groups, indicate the role of these groups in terms of degradability of the title molecule.

4.6 MNPE Docking Analysis towards GABA Receptor

4.6.1 Protein Structure Validation

The validation of the structure of the target protein is an essential step in the drug discovery process [55]. The crystal structure of a human GABA receptor (PDB ID: 4COF) shown in Fig. 10a was done at a resolution of 2.97 Å and was used as the target protein [17]. The target protein contains 5 possible binding sites, namely chains A, B, C, D and E. Each chain is consisted of about five α-helices which are spiral in shape and about 8 β-pleated sheets. Ramachandran plot (Fig. 10b) checked a total number of 1574 residues out of the 1665 amino residues present in the target protein, which is tantamount to about 95% of the total residues. The total number of core regions and outliers are 1546 and 28 respectively, which gave a rise to a percentage outlier of 1.8 %. The Ramachandran plot uses percentage outlier to ascertain the validity of a protein structure. The recommended range for the percentage outlier for a valid protein structure is between 0 to 5 % [56]. Hence, the target protein (PDB ID: 4COF) used for the molecular docking was valid.

4.6.2 Molecular Docking

The five binding sites of the benzamidine molecule, A, B, C, D and E, complexed with the crystal structure of the target protein (PDB ID: 4COF) were used for docking analysis. Benzamidine is an agonist for the human GABA receptor [17] and hence its binding site was used as a reference for the molecular docking analysis. Table 8 lists the molecular docking results of MNPE and human GABA receptor. Binding site C which is the reference site for BEN C in the original crystal structure had the highest total docking score value which implies that MNPE exhibits the best binding affinity towards the target protein within this binding site. The total score value is the sum of the Hydrogen Bond (HB) score, the Steric Interaction (SI) score and the ligand penalty conformation. It was also predicted that the ligand in binding cite C has the lowest ligand conformation penalty value (7.910) and the most negative steric interaction score (-59.781) among the different binding sites. Four types of favorable interactions (Fig. 11) between MNPE and the target protein could be established. The favorable interactions between MNPE and the target protein included conventional hydrogen bonding with amino acids THR 202 and GLN 64, π-π stacking and π-alkyl interactions with PHE 200, TYR 62 and TYR 205, and carbon hydrogen bond with ASP 43 and TYR 157 (Fig. 11).

4.6.3 Binding Mode Conformation

The molecular docking analysis involved the generation of five low energy conformational scenarios known as poses. Unlike regular conformations, a pose structure is dependent on the target protein. Each pose was screened against the target protein in each of the five binding sites, A thru E. The binding mode conformation of MNPE in a binding site C have shown the best binding affinity (Fig. 11). During molecular docking analysis, the molecule orientated itself such that there exist an intramolecular hydrogen bonding between one of the hydrogens of the piperazine ring and the oxygen of the carbonyl group. The comparison between the most stable conformer (B4) and the best binding pose from the molecular docking analysis is depicted in Fig. 12. It was evident that the docked pose and most stable conformer of MNPE were similar with respect to the position of the various functional groups except that the structure of the binding pose is contracted due to the presence of intramolecular hydrogen bonding along with its orientation of the flexible bonds in the molecule. The difference in the structure of the binding pose arises because in molecular docking the molecule would orientate itself such that it best-fit into the binding pocket of the target protein to ensure adequate binding.

4.7 Vibrational Assignments of the IR and Raman Spectra

Understanding the detailed infrared and Raman features of newly synthesized, biologically active molecules is essential for tracing purposes as well as gaining advanced structural comprehension. In order to further elaborate on the vibrational spectral properties of MNPE, the calculated scaled wavenumbers, observed IR, Raman bands and detailed vibrational assignments for MNPE were provided in table 5.

4.7.1 NO_2 Modes

According to literature, the NO_2 stretching modes are normally observed in the regions 1580 ± 80 (asymmetric) and 1330 ± 30 cm^{-1} (symmetric) [57]. For the title compound, NO_2 stretching modes are assigned at 1502, 1310 cm^{-1} in the IR spectrum, 1492, 1308 cm^{-1} in the Raman spectrum and at 1495, 1307 cm^{-1} theoretically with PEDs 66 and 49%. Both the modes possess a high IR intensity and the mode at 1307 cm^{-1} has a high Raman activity. Mary et al. reported the NO_2 stretching modes at 1429, 1363 (DFT), 1435, 1368 (IR), 1435, 1367 cm^{-1} (Raman) [58]. The NO_2 deformation modes (scissoring, out-of-plane wagging, in-plane rocking

and torsion) are expected in the regions 855 ± 40, 760 ± 30, 540 ± 30 and 70 ± 20 cm^{-1}, respectively [57]. The bands at 844, 808 cm^{-1} in the Raman spectrum and 842, 807 and 549 cm^{-1} (DFT) are assigned as the deformation modes of the NO_2 group for MNPE. These modes have 39, 38, 47% PEDs, and the first two modes possess a medium-strength IR and Raman intensities. The reported values of the NO_2 deformations modes are: 778, 692, 533 (DFT), 773, 522 (IR), 773 cm^{-1} (Raman) [58] and at 800, 727, 534 (DFT), 809, 727, 524 cm^{-1} (experimentally) [59].

4.7.2 C-O-C and C=O Modes

The C-O-C stretching vibrations are expected in the ranges, 1310-1110 and 1050-1010 cm^{-1} [57], [60]. In the present case the C-O-C stretching modes are assigned at 1240, 1008 cm^{-1} theoretically with a PED of 40% and correspond experimentally to 1010 cm^{-1} in the IR and 1242 cm^{-1} in the Raman spectra. Mary *et al.* reported the C-O-C stretching modes at 1042, 1016, 982 cm^{-1} in the IR spectrum and at 1135, 1132, 1080, 1046, 1012, 984 cm^{-1} theoretically [61]. Moreover, the C=O stretching mode in MNPE is assigned at 1648 cm^{-1} in IR, 1649 cm^{-1} in Raman and 1655 cm^{-1} theoretically which is in agreement with the expected region of 1750-1600 cm^{-1} [57], [62], [63]. The carbonyl stretching mode is predicted to have minimum coupling from other modes with a PED of 75% and of high infrared and Raman intensities [57].

4.7.3 CH_3 Modes

For the title compound, the CH_3 stretching modes are assigned at 2977, 2944 cm^{-1} in the infrared spectrum, 3032, 2950, 2900 cm^{-1} in the Raman spectrum and in the range 3030-2895 cm^{-1} theoretically. The deformation modes of the methyl groups of the title compound are normally highly coupled with other bending modes. In MNPE the infrared bands observed at 1430 and 1339 cm^{-1} and Raman lines observed at 1428, 1159, 970 cm^{-1} are assigned as CH_3 deformations (Table 5). The corresponding theoretical values are in the range 1443-1338 cm^{-1} (scissoring) and 1161-967 cm^{-1} (rocking) [57].

4.7.4 C-N and C-C Modes

The C-N stretching modes are observed in the range 1300-1000 cm^{-1} [62], [63] and for the title compound these modes are assigned at 1178, 1073 cm^{-1} in the IR spectrum, 1224, 1077 cm^{-1} in the Raman spectrum and at 1220, 1185, 1074 cm^{-1} theoretically with PEDs of 44, 41 and

36%, respectively. El-Azab *et al.* [43] reported the C-N stretching modes at 1232, 1146, 1108, 966 cm^{-1} in the IR spectrum, 1232, 1149, 1108, 967 cm^{-1} in the Raman spectrum and in the range 1235-965 cm^{-1} theoretically. For the title compound the C-C stretching mode is assigned at 904 cm^{-1} in the Raman spectrum and at 902 cm^{-1} theoretically as expected [63].

4.7.5 Piperazine Ring Modes

The CH_2 stretching modes in the piperazine ring could be assigned to 3014, 2977, 2876, 2820 cm^{-1} in the infrared and to 2999, 2981, 2885, 2843 cm^{-1} in the Raman spectra. El-Emam *et al.* [39] reported stretching CH_2 vibrations in the piperazine ring in the range 3033-2834 cm^{-1}. Renjith *et al.* reported the CH_2 stretching modes in the piperazine ring at 2986, 2976, 2965, 2923 cm^{-1} (theoretical), 2990, 2923 cm^{-1} (IR) and 2988, 2924 cm^{-1} (Raman) [64]. The corresponding deformation modes could be assigned to 1363, 1202, 1178, 1092, 1036, 829 cm^{-1} in the IR and to 1452, 1364, 1333, 1242, 1224, 1196, 1091, 1040, 829 cm^{-1} in the Raman spectra. According to H. L. Spell [65] the CH_2 deformation modes associated with the piperazine ring are usually observed ass harp, well defined absorptions at 1380-1345 cm^{-1}, 125-1170 cm^{-1} and 1050-1025 cm^{-1} regions in the infrared spectrum. It prompted us to assign the strong peak observed in the infrared spectrum of MNPE at 1363 cm^{-1} (Fig. 2) to the CH_2 wagging mode of the piperazine ring in agreement with the DFT value (1361 cm^{-1}). Furthermore, another intense band observed at 1036 cm^{-1} in the IR spectrum was assigned to the ring CH_2 rocking vibration, in consistency with previously reported finding da Silva *et al.* [66]. According to H. L. Spell [65], this is one of the key bands useful for the detection of the presence of di-substituted piperazines.

Piperazine ring stretching modes in MNPE could be observed at 1131, 960, 697 cm^{-1} in the ir spectrum and at 1196, 1018, 954, 904, 701 cm^{-1} in the Raman spectrum. The PED analysis predicts these modes in the range 1193-699 cm^{-1}. Renjith *et al.* reported the piperazine ring stretching modes 1099, 985, 930 cm^{-1} in the IR spectrum, 1100, 924, 905 cm^{-1} in the Raman spectrum and 1159, 1098, 1020, 982, 924 and 914 cm^{-1} theoretically [64]. The C-C stretching vibrations in the piperaizne ring were previously reported at 972 and 903 cm^{-1} [58] while the C-N stretching modes were reported in the range 1154-756 cm^{-1} [58].

4.7.6 Phenyl Ring Modes

The C-H stretching modes of the phenyl ring are expected above 3000 cm^{-1} [57] and, for the title compound, the bands at 3118, 3078 cm^{-1} (Raman) and 3120, 3094, 3081 cm^{-1} (DFT) are assigned as the C-H stretching vibrations of the phenyl ring. The phenyl ring stretching modes are assigned at 1574, 1550, 1476, 1288 cm^{-1} in the IR spectrum, 1577, 1392 cm^{-1} in the Raman spectrum and at 1576, 1553, 1473, 1391, 1291 cm^{-1} theoretically which are expected in the region 1250-1600 cm^{-1} [57]. The ring breathing mode of the phenyl ring is assigned at 1010 cm^{-1} in the IR spectrum and at 1008 cm^{-1} theoretically as reported in literature [57], [67]. The reported values of the ring breathing mode of poly substituted phenyl ring at 978 cm^{-1} [43], 1025 cm^{-1} in the Raman spectrum and 1032 cm^{-1} theoretically [68]. The C-H in-plane and out-of-plane bendings of the phenyl ring are expected above and below 1000 cm^{-1} [57] and for the title compound, the bands at 1258, 1073 cm^{-1} (IR), 1077 cm^{-1} (Raman), 1257, 1146, 1074 cm^{-1} (DFT) and 932, 801 cm^{-1} (IR), 935, 799, 789 cm^{-1} (DFT) are assigned as the in-plane and out-of-plane CH deformation modes, respectively.

5. Conclusions

The synthesis and vibrational spectroscopic properties of 1-(4-(3-methoxy-4-nitrophenyl)piperazin-1-yl)ethanone (MNPE) have been accomplished. MEP studies revealed the most reactive sites in the molecule. The low HOMO-LUMO energy gap is associated with the high chemical reactivity and existence of charge transfer within the molecule. ALIE surfaces indicated that significant reactive centers, prone to electrophilic attacks, could be located at carbon atoms of the benzene ring, nitrogen atom of the piperazine moiety and oxygen atoms of the nitro group. Bond dissociation energy values of hydrogen abstraction indicated that MNPE is highly stable in open air and in the presence of oxygen, however, the calculated RDF curves revealed that MNPE is dissociable in aqueous systems. The molecular docking analysis showed that binding site C had the best binding affinity towards the GABA receptor

Acknowledgment

Experimental and computational resources provided by King Fahd University of Petroleum and Minerals (KFUPM) to support this work are appreciated. Support received from Schrödinger Inc. is appreciated. Part of this study was conducted within the projects supported by the Ministry of

Education, Science and Technological Development of Serbia, grant numbers OI 171039 and TR 34019 (project period 2016-2019/20).

References

[1] J. Cai, Y. Lu, L. Gan, Y. Zhang, and C. Zhou, "Recent advance in the research of piperazine-containing compounds as antimicrobial agents," *Chin. J. Antibiot*, 8 (2009) 3.

[2] L. L. Gan, Y. H. Lu, and Zhou C.H., "Advances in the research of piperazine compounds as enzyme inhibitors," *Chin. J. Biochem. Pharm*, vol. 30, no. 6, pp. 127–131, 2009.

[3] Y.-J. Shaw, Y.-T. Yang, J. B. Garrison, N. Kyprianou, and C.-S. Chen, "Pharmacological Exploitation of the α1-Adrenoreceptor Antagonist Doxazosin to Develop a Novel Class of Antitumor Agents That Block Intracellular Protein Kinase B/Akt Activation," *J. Med. Chem.*, vol. 47, no. 18, pp. 4453–4462, 2004.

[4] J. Chen, M. Lu, Y. Jing, and J. Dong, "The synthesis of L-carvone and limonene derivatives with increased antiproliferative effect and activation of ERK pathway in prostate cancer cells," *Bioorg. Med. Chem.*, 14 (2006) 6539-6547.

[5] S. Richter, C. Parolin, and M. Palumbo, "Antiviral properties of quinolone-based drugs," *Drug Targets-Infectious*, 4 (2004) 111-116.

[6] W. J. Watkins, L. Chong, A. Cho, R. Hilgenkamp, M. Ludwikow, N. Garizi, N. Iqbal, J. Barnard, R. Singh, D. Madsen, K. Lolans, O. Lomovskaya, U. Oza, P. Kumaraswamy, A. Blecken, S. Bai, D. J. Loury, D. C. Griffith, and M. N. Dudley, "Quinazolinone fungal efflux pump inhibitors. Part 3: (N-methyl)piperazine variants and pharmacokinetic optimization," *Bioorg. Med. Chem. Lett.*, vol. 17, no. 10, pp. 2802–2806, May 2007.

[7] M. Kimura, T. Masuda, K. Yamada, N. Kawakatsu, N. Kubota, M. Mitani, K. Kishii, M. Inazu, Y. Kiuchi, K. Oguchi, and T. Namiki, "Antioxidative activities of novel diphenylalkyl piperazine derivatives with high affinities for the dopamine transporter," *Bioorg. Med. Chem. Lett.*, vol. 14, no. 16, pp. 4287–4290, 2004.

[8] R. A. Smits, H. D. Lim, A. Hanzer, O. P. Zuiderveld, E. Guaita, M. Adami, G. Coruzzi, R. Leurs, and I. J. P. Esch, "Fragment Based Design of New H 4 Receptor−Ligands with Anti-inflammatory Properties in Vivo," *J. Med. Chem.*, vol. 51, no. 8, pp. 2457–2467, 2008.

[9] W. Cunico, C. R. B. Gomes, M. Moreth, D. P. Manhanini, I. H. Figueiredo, C. Penido, M. G. M. O. Henriques, F. P. Varotti, and A. U. Krettli, "Synthesis and antimalarial activity of hydroxyethylpiperazine derivatives," *Eur. J. Med. Chem.*, vol. 44, no. 3, pp. 1363–1368, 2009.

[10] J. Penjišević, V. Šukalović, D. Andrić, S. Kostić-Rajačić, V. Šoškić, and G. Roglić, "1-Cinnamyl-4-(2-methoxyphenyl)piperazines," *Arch. Pharm. (Weinheim).*, vol. 340, no. 9, pp. 456–465, 2007.

[11] D. S. Wishart, C. Knox, A. C. Guo, S. Shrivastava, M. Hassanali, P. Stothard, Z. Chang, and J. Woolsey, "DrugBank: a comprehensive resource for in silico drug discovery and exploration.," *Nucleic Acids Res.*, vol. 34, no. Database issue, pp. D668–D672, 2006.

[12] A. Golubović, B. Abramović, M. Šćepanović, M. Grujić-Brojčin, S. Armaković, I.

Veljković, B. Babić, Z. Dohčević-Mitrović, and Z. V Popović, “Improved efficiency of sol–gel synthesized mesoporous anatase nanopowders in photocatalytic degradation of metoprolol,” *Mater. Res. Bull.*, vol. 48, no. 4, pp. 1363–1371, 2013.

[13] R. Ma, B. Wang, S. Lu, Y. Zhang, L. Yin, J. Huang, S. Deng, Y. Wang, and G. Yu, “Characterization of pharmaceutically active compounds in Dongting Lake, China: Occurrence, chiral profiling and environmental risk,” *Sci. Total Environ.*, vol. 557–558, pp. 268–275, Jul. 2016.

[14] S. J. Armaković, S. Armaković, N. L. Finčur, F. Šibul, D. Vione, J. P. Šetrajčić, and B. F. Abramović, “Influence of electron acceptors on the kinetics of metoprolol photocatalytic degradation in TiO 2 suspension. A combined experimental and theoretical study,” *RSC Adv*, vol. 5, no. 67, pp. 54589–54604, 2015.

[15] D. Šojić, V. Despotović, D. Orčić, E. Szabó, E. Arany, S. Armaković, E. Illés, K. Gajda-Schrantz, A. Dombi, T. Alapi, E. Sajben-Nagy, A. Palágyi, C. Vágvölgyi, L. Manczinger, L. Bjelica, and B. Abramović, “Degradation of thiamethoxam and metoprolol by UV, O3 and UV/O3 hybrid processes,” *J. Hydrol.*, vol. 472–473, pp. 314–327, 2012.

[16] B. Abramović, S. Kler, D. Šojić, M. Laušević, T. Radović, and D. Vione, “Photocatalytic degradation of metoprolol tartrate in suspensions of two TiO_2-based photocatalysts with different surface area. Identification of intermediates and proposal of degradation pathways,” *J. Hazard. Mater.*, vol. 198, pp. 123–132, 2011.

[17] P. S. Miller and A. R. Aricescu, “Crystal structure of a human GABAA receptor,” *Nature*, 512 (2014) 270-275.

[18] P. R. Schofield, M. G. Darlison, N. Fujita, D. R. Burt, F. A. Stephenson, H. Rodriguez, L. M. Rhee, J. Ramachandran, V. Reale, T. A. Glencorse, P. H. Seeburg, and E. A. Barnard, “Sequence and functional expression of the GABAA receptor shows a ligand-gated receptor super-family,” *Nature*, vol. 328, no. 6127, pp. 221–227, Jul. 1987.

[19] W. Sieghart, “GABAA receptors: ligand-gated Cl− ion channels modulated by multiple drug-binding sites,” *Trends Pharmacol. Sci.*, vol. 13, pp. 446–450, Jan. 1992.

[20] a) A. J. Pawson, J. L. Sharman, H. E. Benson, E. Faccenda, S. P. H. Alexander, O. P. Buneman, A. P. Davenport, J. C. McGrath, J. A. Peters, C. Southan, M. Spedding, W. Yu, and A. J. Harmar, “The IUPHAR/BPS Guide to PHARMACOLOGY: An expert-driven knowledgebase of drug targets and their ligands,” *Nucleic Acids Res.*, vol. 42, no. D1, pp. 1098–1106, 2014. b) A. O. Ba-Salema, M. N. Shaikh, N. Ullah and M. Faiz, "Synthesis and magnetic relaxation properties of new Gd(III) complexes derived from DTPA-bis(amide) conjugates of arylpiperazinyl amines," *Inorg. Chem. Commun.*, vol. 56, pp. 5-7, 2015.

[21] G. E. S. M. J. Frisch, G. W. Trucks, H. B. Schlegel, B. M. M. A. Robb, J. R. Cheeseman, G. Scalmani, V. Barone, H. P. H. G. A. Petersson, H. Nakatsuji, M. Caricato, X. Li, M. H. A. F. Izmaylov, J. Bloino, G. Zheng, J. L. Sonnenberg, T. N. M. Ehara, K. Toyota, R. Fukuda, J. Hasegawa, M. Ishida, J. Y. Honda, O. Kitao, H. Nakai, T. Vreven, J. A. Montgomery, E. B. J. E. Peralta, F. Ogliaro, M. Bearpark, J. J. Heyd, J. N. K. N. Kudin, V. N. Staroverov, T. Keith, R. Kobayashi, J. T. K. Raghavachari, A. Rendell, J. C. Burant, S. S. Iyengar, J. B. C. M. Cossi, N. Rega, J. M. Millam, M. Klene, J. E. Knox, R. E. S. V. Bakken, C. Adamo, J. Jaramillo, R. Gomperts, J. W. O. O. Yazyev, A. J. Austin, R. Cammi, C. Pomelli, G. A. V. R. L. Martin, K. Morokuma, V. G. Zakrzewski, A. D. D. P. Salvador, J. J. Dannenberg, S. Dapprich, J. C. O. Farkas, J. B. Foresman, J. V. Ortiz, and and D. J. Fox, “Gaussian 09, Revision D.01,” *Gaussian, Inc. Wallingford CT*. 2013.

[22] A. Irfan, R. Jin, A. G. Al-Sehemi, and A. M. Asiri, "Quantum chemical study of the donor-bridge-acceptor triphenylamine based sensitizers," *Spectrochim. Acta Part A Mol. Biomol. Spectrosc.*, vol. 110, pp. 60–66, 2013.
[23] A. Irfan, A. G. Al-Sehemi, and M. S. Al-Assiri, "The effect of donors–acceptors on the charge transfer properties and tuning of emitting color for thiophene, pyrimidine and oligoacene based compounds," *J. Fluor. Chem.*, vol. 157, pp. 52–57, 2014.
[24] E. F. J.B. Foresman, *Exploring Chemistry with Electronic Structure Methods: A Guide to Using Gaussian*, no. 1 TS-CrossRef Metadata Search. Pittsburg: Gaussian Inc., 1996.
[25] A. A. Al-Saadi and J. Laane, "Ab initio and DFT calculations for the structure and vibrational spectra of cyclopentene and its isotopomers," *J. Mol. Struct.*, vol. 830, no. 1–3, pp. 46–57, 2007.
[26] R. Dennington, T. Keith, and J. Millam, "GaussView." Semichem Inc, Shawnee Mission KS, 2009.
[27] C. V. A. J.M.L. Martin, "GAR2PED," vol. 44, no. 2. University of Antwerp, Belgium, 2007.
[28] A. D. Bochevarov, E. Harder, T. F. Hughes, J. R. Greenwood, D. A. Braden, D. M. Philipp, D. Rinaldo, M. D. Halls, J. Zhang, and R. A. Friesner, "Jaguar: A high-performance quantum chemistry software program with strengths in life and materials sciences," *Int. J. Quantum Chem.*, vol. 113, no. 18, pp. 2110–2142, 2013.
[29] D. Shivakumar, J. Williams, Y. Wu, W. Damm, J. Shelley, and W. Sherman, "Prediction of Absolute Solvation Free Energies using Molecular Dynamics Free Energy Perturbation and the OPLS Force Field," *J. Chem. Theory Comput.*, vol. 6, no. 5, pp. 1509–1519, 2010.
[30] Z. Guo, U. Mohanty, J. Noehre, T. K. Sawyer, W. Sherman, and G. Krilov, "Probing theα-Helical Structural Stability of Stapled p53 Peptides: Molecular Dynamics Simulations and Analysis," *Chem. Biol. Drug Des.*, vol. 75, no. 4, pp. 348–359, Apr. 2010.
[31] K. J. Bowers, F. D. Sacerdoti, J. K. Salmon, Y. Shan, D. E. Shaw, E. Chow, H. Xu, R. O. Dror, M. P. Eastwood, B. A. Gregersen, J. L. Klepeis, I. Kolossvary, and M. A. Moraes, "Molecular dynamics---Scalable algorithms for molecular dynamics simulations on commodity clusters," in *Proceedings of the 2006 ACM/IEEE conference on Supercomputing - SC '06*, 2006, p. 84.
[32] D. E. Shaw Research, "Schrödinger Release 2015-4: Desmond Molecular Dynamics System." 2015.
[33] A. D. Becke, "Density-functional thermochemistry. III. The role of exact exchange," *J. Chem. Phys.*, vol. 98, no. 7, pp. 5648–5652, 1993.
[34] J. L. Banks, H. S. Beard, Y. Cao, A. E. Cho, W. Damm, R. Farid, A. K. Felts, T. A. Halgren, D. T. Mainz, J. R. Maple, R. Murphy, D. M. Philipp, M. P. Repasky, L. Y. Zhang, B. J. Berne, R. A. Friesner, E. Gallicchio, and R. M. Levy, "Integrated Modeling Program, Applied Chemical Theory (IMPACT)," *J. Comput. Chem.*, vol. 26, no. 16, pp. 1752–1780, 2005.
[35] H. J. C. Berendsen, J. P. M. Postma, W. F. van Gunsteren, and J. Hermans, "Interaction Models for Water in Relation to Protein Hydration," in *Intermolecular Forces*, vol. 14, B. Pullman, Ed. Dordrecht: Springer Netherlands, 1981, pp. 331–342.
[36] T. Knudsen, Bjarne Knudsen, "CLC Drug Discovery Workbench." pp. 1–367, 2016.
[37] G. J. Kleywegt and T. A. Jones, "Phi/Psi-chology," *Structure*, vol. 4, no. 12, pp. 1395–1400, 1996.
[38] I. P. Holmes, Y. Bergman, G. E. Lunniss, M. Nikac, N. Chol, C. F. Hemley, S. R. Walker,

R. C. Foitzik, D. Ganame, and R. Lessene, US 20130022594, 2013.

[39] A. A. El-Emam, A.-M. S. Al-Tamimi, K. A. Al-Rashood, H. N. Misra, V. Narayan, O. Prasad, and L. Sinha, "Structural and spectroscopic characterization of a novel potential chemotherapeutic agent 3-(1-adamantyl)-1-{[4-(2-methoxyphenyl)piperazin-1-yl]methyl}-4-methyl-1H-1,2,4-triazole-5(4H)-thione by first principle calculations," *J. Mol. Struct.*, vol. 1022, pp. 49–60, 2012.

[40] K. S. Resmi, Y. S. Mary, H. T. Varghese, C. Y. Panicker, M. Pakosińska-Parys, and C. van Alsenoy, "Spectral investigations, DFT computations and molecular docking studies of 1,7,8,9-tetrachloro-10,10-dimethoxy-4-{3-[4-(2-methylphenyl)piperazin-1-yl]propyl}-4-azatricyclo[5.2.1.02,6]dec-8-ene-3,5-dione," *J. Mol. Struct.*, vol. 1098, pp. 130–145, 2015.

[41] Z. Karczmarzy and W. Malinka, "Crystal Structure of 4,6-Dimethyl-2-[4-(2,3-dichlorophenyl)piperazin-1-ylmethyl]isothiazolo[5,4-b]pyridin-3(2H)-one," *Anal. Sci. X-ray Struct. Anal. Online*, vol. 23, pp. x151–x152, 2007.

[42] Y. Sheena Mary, T. S. Yamuna, C. Y. Panicker, H. S. Yathirajan, M. S. Siddegowda, A. a Al-Saadi, C. Van Alsenoy, and J. A. War, "Vibrational spectroscopic studies and molecular docking of 10,10-Dimethylanthrone.," *Spectrochim. Acta. A. Mol. Biomol. Spectrosc.*, vol. 135, pp. 652–61, 2015.

[43] A. S. El-Azab, Y. Sheena Mary, C. Yohannan Panicker, A. A.-M. Abdel-Aziz, M. A. El-Sherbeny, and C. van Alsenoy, "DFT and experimental (FT-IR and FT-Raman) investigation of vibrational spectroscopy and molecular docking studies of 2-(4-oxo-3-phenethyl-3,4-dihydroquinazolin-2-ylthio)-N-(3,4,5-trimethoxyphenyl) acetamide," *J. Mol. Struct.*, vol. 1113, pp. 133–145, 2016.

[44] Y. Sheena Mary, K. Raju, C. Y. Panicker, A. A. Al-Saadi, T. Thiemann, and C. van Alsenoy, "Molecular conformational analysis, vibrational spectra, NBO analysis and first hyperpolarizability of (2E)-3-phenylprop-2-enoic anhydride based on density functional theory calculations," *Spectrochim. Acta Part A Mol. Biomol. Spectrosc.*, vol. 128, pp. 638–646, 2014.

[45] C. Y. Panicker, H. T. Varghese, P. S. Nayak, B. Narayana, B. K. Sarojini, H. K. Fun, J. A. War, S. K. Srivastava, and C. van Alsenoy, "Infrared spectrum, NBO, HOMO–LUMO, MEP and molecular docking studies (2E)-3-(3-nitrophenyl)-1-[4-piperidin-1-yl]prop-2-en-1-one," *Spectrochim. Acta Part A Mol. Biomol. Spectrosc.*, vol. 148, pp. 18–28, 2015.

[46] P. Sjoberg, J. S. Murray, T. Brinck, and P. Politzer, "Average local ionization energies on the molecular surfaces of aromatic systems as guides to chemical reactivity," *Can. J. Chem.*, vol. 68, no. 8, pp. 1440–1443, 1990.

[47] P. Politzer, F. Abu-Awwad, and J. S. Murray, "Comparison of density functional and Hartree-Fock average local ionization energies on molecular surfaces," *Int. J. Quantum Chem.*, vol. 69, no. 4, pp. 607–613, 1998.

[48] A. Michalak, F. Proft, P. Geerlings, and R. F. Nalewajski, "Fukui Functions from the Relaxed Kohn−Sham Orbitals," *J. Phys. Chem. A*, vol. 103, no. 6, pp. 762–771, 1999.

[49] A. E. R. E.D. Glendening J.E. Carpenter, F.Weinhold, "NBO Version 3.1," vol. 81 TS-C, no. 32. Gaussian Inc., 2003.

[50] A. B. T. Andersson E. Evertsson, "Prediction of drug candidates sensitivity toward autoxidation:Computational estimation of C-H dissociation energies of carbon centered radicals," *J. Pharm. Sci.*, vol. 103, p. 1949–1955.

[51] P. Lienard, J. Gavartin, G. Boccardi, and M. Meunier, "Predicting drug substances

autoxidation," *Pharm. Res.*, vol. 32, no. 1, pp. 300–310, 2015.
[52] Y.-R. Luo, *Handbook of bond dissociation energies in organic compounds*. Boca Raton, FL: CRC Press, 2003.
[53] J. S. Wright, H. Shadnia, and L. L. Chepelev, "Stability of carbon-centered radicals: Effect of functional groups on the energetics of addition of molecular oxygen," *J. Comput. Chem.*, vol. 30, no. 7, pp. 1016–1026, May 2009.
[54] R. V. Vaz, J. R. B. Gomes, and C. M. Silva, "Molecular dynamics simulation of diffusion coefficients and structural properties of ketones in supercritical CO_2 at infinite dilution," *J. Supercrit. Fluids*, vol. 107, pp. 630–638, Jan. 2016.
[55] M. E. Bunnage, A. M. Gilbert, L. H. Jones, and E. C. Hett, "Know your target, know your molecule," *Nat. Chem. Biol.*, vol. 11, no. 6, pp. 368–372, 2015.
[56] G. J. Kleywegt and T. A. Jones, "Phi/Psi-chology: Ramachandran revisited," *Structure*, vol. 4, no. 12, pp. 1395–1400, 1996.
[57] N. P. G. Roeges, *A guide to the complete interpretation of infrared spectra of organic structures*. Wiley, 1994.
[58] Y. Sheena Mary, K. Raju, T. E. Bolelli, I. Yildiz, H. I. S. Nogueira, C. M. Granadeiro, and C. van Alseony, "FT-IR, FT-Raman, surface enhanced Raman scattering and computational study of 2-(p-fluorobenzyl)-6-nitrobenzoxazole," *J. Mol. Struct.*, vol. 1012, pp. 22–30, 2012.
[59] H. T. V. C.Y. Panicker L. Usha Kumari, T. Ertan, I. Yildiz, C.M. Granadeiro, H.I.S. Nogueira, Y.S. Mary, "FT-IR, FT-Raman, SERS spectra and Computational calculations of 4-Ethyl-N-(2'-hydroxy-5'-nitrophenyl)benzamide," *J. Raman Spectrosc.*, vol. 41, p. 381–390., 2010.
[60] B. Smith, *Infrared spectral interpretation:A systematic approach*, vol. 36 TS-C, no. 10. Washington, DC: CRC Press, 1999.
[61] Y. Sheena Mary, C. Yohannan Panicker, P. L. Anto, M. Sapnakumari, B. Narayana, and B. K. Sarojini, "Molecular structure, FT-IR, NBO, HOMO and LUMO, MEP and first order hyperpolarizability of (2E)-1-(2,4-Dichlorophenyl)-3-(3,4,5-trimethoxyphenyl)prop-2-en-1-one by HF and density functional methods," *Spectrochim. Acta Part A Mol. Biomol. Spectrosc.*, vol. 135, pp. 81–92, 2015.
[62] L. H. D. N.B. Colthup S.E. Wiberly, *Introduction to IR and Raman Spectroscopy*. New York: Academic Press TS - CrossRef Metadata Search M4 - Citavi, 1990.
[63] R. M. (Robert M. Silverstein, F. X. Webster, D. J. Kiemle, and D. L. (David L. Bryce, *Spectrometric identification of organic compounds*. .
[64] R. Renjith, Y. Sheena Mary, C. Yohannan Panicker, H. T. Varghese, M. Pakosinska-Parys, C. van Alsenoy, and A. A. Al-Saadi, "Spectroscopic (FT-IR, FT-Raman) investigations and quantum chemical calculations of 1,7,8,9-tetrachloro-10,10-dimethoxy-4-{3-4-(3-methoxyphenyl)piperazin-1-ylpropy l}-4-azatricyclo5.2.1.0(2,6)dec-8-ene-3,5-dione," *Spectrochim. Acta. A. Mol. Biomol. Spectrosc.*, vol. 129, pp. 438–450, 2014.
[65] H. L. Spell, "Determination of piperazine rings in ethyleneamines, poly(ethyleneamine), and polyethylenimine by infrared spectrometry," *Anal. Chem.*, vol. 41, no. 7, pp. 902–905, 2002.
[66] S. P. M.A.S. da Silva T. Francisco, F.O.N. Da Silva, A.A. Batista, J. Ellena, I.M.M. Varvalho, J.R. de Sousa, F.A. Dias-Filho, E. Longhinotti, I.C.N. Diogenes, "A novel and simple synthetic route for a piperazine derivative," *J. Braz. Chem. Soc*, vol. 21, pp. 1754–1759.

[67] G. Varsanyi, *Assignments for Vibrational Spectra of Seven Hundred Benzene Derivatives*, vol. 51 TS-C, no. 2. New York: Wiley, 1974.

[68] A. Raj, Y. Sheena Mary, C. Yohannan Panicker, H. T. Varghese, and K. Raju, "IR, Raman, SERS and computational study of 2-(benzylsulfanyl)-3,5-dinitrobenzoic acid," *Spectrochim. Acta. A. Mol. Biomol. Spectrosc.*, vol. 113, pp. 28–36, 2013.

LIST OF TABLES

Table 1. Conformations and relative energies of the title compound

Conformation	Relative energy (kcal/mol)	
Computational Method	B3LYP/6-311G(d,p)	B3LYP/6-311++G(d,p)
A1	0.127	0.137
A2	0.107	0.126
A3	0.434	0.474
A4	0.174	0.188
B1	0.283	0.298
B2	0.286	0.319
B3	0.258	0.29
B4	0.000	0.000
C1	1.271	1.591
C2	1.5	1.837
C3	1.627	1.975
C4	0.89	1.236
D1	1.205	1.523
D2	1.475	1.811
D3	1.645	1.995
D4	0.972	1.318

Table 2. Bond lengths of selected atoms

Models	N_{15}-O_{37}	N_1-C_6	C_9-O_{13}	O_{13}-O_{37}	N_1-C_7	N_4-C_{16}	C_{16}-O_{17}
A1	1.224	1.462	1.346	2.665	1.399	1.378	1.222
	(1.223)	(1.464)	(1.346)	(2.64)	(1.398)	(1.379)	(1.22)
A2	1.225	1.461	1.345	2.644	1.398	1.377	1.222
	(1.223)	(1.464)	(1.345)	(2.622)	(1.397)	(1.379)	(1.22)
A3	1.232	1.463	1.347	2.651	1.399	1.378	1.222
	(1.23)	(1.465)	(1.346)	(2.627)	(1.398)	(1.378)	(1.219)
A4	1.232	1.46	1.346	2.657	1.397	1.378	1.222
	(1.231)	(1.463)	(1.346	(2.634)	(1.396)	(1.379)	(1.219)
B1	1.224	1.462	1.347	2.666	1.399	1.378	1.222
	(1.223	(1.465)	(1.347)	(2.64)	(1.399)	(1.379)	(1.219)
B2	1.225	1.461	1.346	2.643	1.397	1.378	1.222
	(1.223	(1.464	(1.346	(2.621)	(1.397)	(1.379)	(1.219)
B3	1.232	1.462	1.346	2.651	1.398	1.378	1.222
	(1.223	(1.465)	(1.346)	(2.627)	(1.398)	(1.379)	(1.22)
B4	1.232	1.46	1.346	2.657	1.397	1.377	1.222
	(1.231)	(1.463	(1.345	(2.635)	(1.397)	(1.379)	(1.22)
C1	1.23	1.456	1.353	2.888	1.394	1.378	1.222
	(1.229)	(1.458)	(1.354)	(2.864)	(1.393	(1.379)	(1.219)
C2	1.23	1.456	1.352	2.89	1.396	1.378	1.222
	(1.229)	(1.458)	(1.353)	(2.865)	(1.395)	(1.379)	(1.22)
C3	1.23	1.456	1.354	2.882	1.393	1.378	1.222
	(1.228)	(1.458)	(1.355)	(2.858)	(1.392)	(1.379)	(1.219)
C4	1.23	1.455	1.352	2.896	1.394	1.378	1.222
	(1.228	(1.457)	(1.352)	(2.877)	(1.393)	(1.379)	(1.22)
D1	1.23	1.456	1.353	2.888	1.394	1.378	1.222
	(1.229	(1.458	(1.354)	(2.864)	(1.393)	(1.379)	(1.219)
D2	1.23	1.456	1.353	2.888	1.396	1.378	1.222
	(1.229)	(1.458)	(1.353)	(2.864)	(1.395)	(1.379)	(1.22)
D3	1.23	1.456	1.354	2.882	1.393	1.378	1.222
	(1.228)	(1.458)	(1.354)	(2.859)	(1.392)	(1.379)	(1.219)
D4	1.23	1.455	1.352	2.897	1.394	1.378	1.222
	(1.228)	(1.457)	(1.352)	(2.877)	(1.394	(1.379)	(1.22)

Table 3. Bond angles of selected atoms of the conformation

Model	O_1-N_2-O_3	O_3-N_2-C_4	C_8-C_7-N_{10}	C_{15}-N_{10}-C_{11}	C_{12}-N_{13}-C_{16}	O_{17}-C_{16}-C_{18}
A1	124.2	117	122.1	112.1	119.6	121
	(124.4)	(116.9)	(122.2)	(112.2)	(119.5)	(121)
A2	124.1	117	120.5	112.3	119.9	121
	(124.2)	(117)	(120.5)	(112.4)	(119.7)	(121.1)
A3	124.2	118.8	120	112.1	119.7	121
	(124.3)	(118.8)	(119.9)	(112.1)	(119.5)	(121)
A4	124.1	118.8	121.5	112.3	119.7	121
	(124.3)	(118.8)	(121.5)	(112.4)	(119.5)	(121)
B1	124.3	117	122	112.1	125.9	121
	(124.4)	(116.9)	(122.1)	(112.2)	(126.2)	(121)
B2	124.1	117	120.3	112.2	125.9	121
	(124.2)	(116.9)	(120.3)	(112.3)	(126.3)	(121)
B3	124.2	118.8	119.9	112.1	125.9	121
	(124.3)	(118.8)	(119.9)	(112.2)	(126.3)	(121)
B4	124.1	118.9	121.4	112.4	126.2	121
	(124.3)	(118.8	(121.4	(112.4	(126.5	(121.1
C1	123.9	117.9	122.1	112.4	119.7	121
	(124)	(117.8)	(122.2)	(112.6)	(119.5)	(121)
C2	123.9	117.9	120.5	112.3	119.8	121
	(124)	(117.8)	(120.5)	(112.3)	(119.6)	(121)
C3	123.9	118.2	121.3	112.6	119.8	121
	(124)	(118.1)	(121.3)	(112.7)	(119.6)	(121.1)
C4	123.9	118.1	121.8	112.5	119.7	121
	(124)	(118.1)	(121.8)	(112.6)	(119.6)	(121)
D1	123.9	117.9	122	112.4	125.9	121
	(124)	(117.9)	(122.1)	(112.6)	(126.2)	(121.1)
D2	123.9	117.9	120.5	112.3	126.1	121
	(124)	(117.8)	(120.5)	(112.3)	(126.4)	(121.1)
D3	123.9	117.9	121.7	112.7	119.9	121
	(124)	(118.1)	(121.2)	(112.8)	(126.5)	(121.1))
D4	123.9	118.1	121.7	112.5	126.1	121
	(124)	(118.1)	(121.7)	(112.5)	(126.4)	(121)

Table 4. Dihedral angles of some selected atoms in the 16 possible conformations

Model	O_{37}-N_{15}-C_{10}-C_9	O_{36}-N_{15}-C_{10}-C_{11}	C_8-C_7-N_1-C_6	C_5-N_4-C_{16}-C_{18}
A1	23.37	23.9	-6.6	6.59
	(27.43)	(28.65)	(-5.22)	(8.24)
A2	19.28	20.68	42.89	4.52
	(23.67)	(25.54)	(42.51)	(5.78)
A3	22.44	21.35	44.59	6.48
	(25.84)	(27.59)	(43.7)	(7.9)
A4	22.38	21.86	-6.21	6.29
	(27.04)	(25.64)	(-5.07)	(7.85)
B1	23.55	24.14	-6.76	-175.8
	(27.71)	(28.97)	(-5.34)	(-175.26)
B2	19.48	20.85	42.84	-175.95
	(23.84)	(25.7)	(42.52)	(-175.38)
B3	22.19	21.08	44.13	-176.21
	(27.26)	(25.51)	(43.33)	(-175.46)
B4	22.34	21.84	-5.87	-176.34
	(27)	(25.61)	(-4.74)	(-176.40)
C1	26.62	22.96	-4.8	6.86
	(29.64)	(26.43)	(-4.09)	-8.24
C2	26.62	23.89	41.91	5.88
	(29.66)	(27.34)	(41.93)	(7.1)
C3	23.08	25.81	31.67	6.57
	(28.86)	(26.65)	(-1.61)	(-4.96)
C4	23.8	27.33	-6.29	5.87
	(26.77)	(29.65)	(-5.51)	(7.22)
D1	26.67	23.03	-4.83	-175.52
	(29.65)	(26.45)	(-4.03)	(-175.11)
D2	26.56	23.81	40.98	-176.5
	(29.58)	(23.81)	(40.8)	(-175.87)
D3	23.1	25.84	31.17	-175.84
	(28.72)	(26.52)	(-2.22)	(-187.62)
D4	23.83	27.37	-5.88	-176.19
	(26.83)	(29.71)	(-5.08)	(-176.64)

Table 5. Calculated scaled wave numbers, observed IR, Raman bands and assignments of the title compound

B3LYP/6-311++G(d,p) (5D, 7F)			IR	Raman	Assignments[a]
υ(cm^{-1})	IR_I	R_A	υ(cm^{-1})	υ(cm^{-1})	
3120	1.69	44.38			υCHI(99)
3094	4.66	112.93	-	3118	υCHI(99)
3081	4.65	38.68	-	-	υCHI(98)
3030	6.99	86.1	-	3078	υCH_3(99)
3024	13.8	124.33	-	3032	υCH_3(91)
3014	13.84	97.07	-	-	υCH_2(97)
3013	5.46	72.2	3014	-	υCH_2(98)
3011	8.77	42.83	-	-	υCH_2(95)
2979	15.07	47.35	-	2999	υCH_2(96)
2976	10.16	43.68	2977	2981	υCH_3(99)
2956	29.15	42.82	2977	-	υCH_3(100)
2920	6.4	158.49	2944	2950	υCH_3(100)
2895	42.63	152.5	-	-	υCH_3(100)
2887	55.9	104.31	-	2900	υCH_2(93)
2877	42.61	71.25	-	2885	υCH_2(92)
2841	69.12	267.53	2876	-	υCH_2(95)
2838	26.23	25.36	-	2843	υCH_2(95)
1655	417.22	20.08	2820	-	υC=O(75)
1576	492.6	212.72	1648	1649	υPhI(59), δCHI(14)
1553	252.25	41.74	1574	1577	υPhI(41), υNO_2(16)
1495	175.89	31.98	1550	-	υNO_2(66)
1473	65.07	18.48	1502	1492	δCHI(28), υPhI(49)
1448	6.46	20.87	1476	-	δCH_2(83)
1443	11.35	3.31	-	1452	δCH_2(48), δCH_3(37)
1441	49.44	5.98	-	-	δCH_3(56), δCH_2(27)
1438	9.44	11.6	-	-	δCH_3(99)
1437	20.68	3.64	-	-	δCH_2(68), δCH_3(23)
1432	5.59	5.86	-	-	δCH_2(84)
1429	24.57	0.68	-	-	δCH_3(56), δCH_2(19)
1427	5.64	10.67	1430	1428	δCH_3(51), δCH_2(39)

1418	11.1	6.29	-	-	$\delta CH_3(78)$, $\delta CH_2(14)$
1396	272.94	4.57	-	-	$\upsilon CN(41)$, $\delta CH_2(20)$, $\upsilon PhII(11)$
1391	51.48	25.46	1400	-	$\delta CH_3(22)$, $\upsilon PhI(52)$, $\delta CHI(19)$
1361	29.39	8.14	-	1392	$\delta CH_2(62)$
1355	15.77	6.35	1363	1364	$\delta CH_2(73)$
1343	21.43	2.26	-	-	$\delta CH_2(51)$, $\upsilon CN(11)$
1338	15.45	4.95	1339	-	$\delta CH_3(62)$, $\delta CH_2(11)$
1335	4.93	21.07	1339	-	$\delta CH_2(53)$, $\delta CH_3(17)$
1319	13.94	25.14	-	1333	$\delta CH_2(75)$
1307	369.53	605.65	-	-	$\upsilon NO_2(49)$, $\upsilon CN(11)$, $\upsilon PhI(20)$, $\delta CH2(10)$
1291	212.78	91.72	1310	1308	$\upsilon PhI(45)$, $\upsilon NO_2(10)$
1261	75.88	11.49	1288	-	$\delta CH_2(53)$, $\upsilon PhII(17)$
1257	37.56	12.93	-	-	$\delta CHI(46)$, $\upsilon PhI(13)$
1240	282.66	168.39	1258	-	$\upsilon CO(40)$, $\delta CH_2(43)$
1220	268.29	63.25	-	1242	$\delta CH_2(39)$, $\upsilon CN(44)$
1198	46.22	18.12	-	1224	$\delta CH_2(41)$, $\upsilon PhII(14)$
1193	144.21	11.38	1202	1196	$\delta CH_2(48)$, $\upsilon PhII(45)$
1185	231.16	9.44	-	1196	$\delta CH_2(46)$, $\upsilon CN(41)$
1161	3.96	8.7	1178	-	$\delta CH_3(53)$, $\delta CHI(10)$, $\upsilon PhI(11)$
1146	6.14	7.25	-	1159	$\delta CHI(40)$, $\delta CH_3(19)$, $\upsilon PhI(15)$
1128	41.36	4.7	-	-	$\upsilon PhII(68)$
1119	0.76	2	1131	-	$\delta CH_3(94)$
1088	6.79	3.47	-	-	$\delta CH_2(40)$, $\tau PhII(10)$, $\upsilon CN(11)$
1074	112.68	77.08	1092	1091	$\upsilon CN(36)$, $\delta CHI(40)$, $\upsilon PhI(11)$
1034	8.76	5.27	1073	1077	$\delta CH_2(50)$, $\delta CH_3(10)$, $\delta PhII(10)$
1027	11.45	3.91	1036	1040	$\delta CH_2(56)$, $\upsilon PhII(13)$
1020	26.42	54.01	-	-	$\upsilon PhII(52)$, $\upsilon CO(11)$
1009	2.46	0.67	-	1018	$\delta CH_3(76)$, $\gamma C{=}O(18)$
1008	48.37	18.85	-	-	$\upsilon CO(40)$, $\upsilon PhI(45)$
967	72.77	0.68	1010	-	$\delta CH_3(43)$, $\upsilon PhII(16)$
956	100.35	0.76	-	970	$\upsilon PhII(56)$, $\delta PhI(22)$
942	8.18	1.5	960	954	$\upsilon PhII(53)$, $\delta PhI(24)$
935	9.15	0.37	-	-	$\gamma CHI(86)$
902	5.74	2.35	932	-	$\upsilon CC(44)$, $\upsilon PhII(44)$

842	12.39	24.42	-	904	δNO_2(39), δPhI(19), υPhII(13)
827	6.2	4.32	-	844	δCH_2(62)
807	17.69	14.09	829	829	δNO_2(38), υPhII(12)
799	40.12	1	-	808	γCHI(51), τPhI(21), γCN(11)
789	1.93	5.3	801	-	γCHI(54), γCO(10), τCN(18), τPhI(12)
733	12.62	2.57	-	-	γCN(54), γCHI(21), τPhI(10)
699	10.3	22.31	728	731	υPhII(42), γCN(12)
692	4.53	3.28	697	701	δPhI(40), τPhI(25)
680	8.5	8.97	-	-	τPhI(41), γCN(12)
646	15.24	3.83	-	-	γCN(18), δPhI(15), γCO(19), δPhII(24)
627	8.13	1.7	651	650	γCO(26), γCN(15), τPhI(15)
594	6.65	4.37	620	620	δC=O(43), δPhII(10), δCN(10)
578	9.37	3.56	592	596	γC=O(20), δC=O(17), δPhII(38)
567	7.9	1.44	-	-	γC=O(46), δCH_3(31)
549	4	7.1	566	567	δPhI(25), δNO_2(47)
497	1.49	2.09	-	-	δCN(25), δPhII(24), δPhI(18)
461	0.22	0.91	-	501	δCN(46), δPhII(11), τPhI(10)
457	3.35	1.7	-	464	δPhII(44), δCN(10)
452	9.7	7.8	457	-	τPhI(44), γCN(25)
416	2.42	5.7	-	444	δCN(38), τPhI(20)
400	4.3	5.19	414	414	δCO(39), δCN(23)
381	1.27	1.48	-	-	τPhII(60)
362	1.24	0.56	-	-	δPhII(27), δPhI(38), δCN(15)
305	1.32	7.66	-	-	τPhI(20), γCN(27), δCN(10)
289	11.08	0.62	-	306	τPhII(38), δCN(39)
273	20.06	4.46	-	286	τPhII(41), γCN(12), δCN(24)
257	3.19	2.58	-	-	τCH_3(46), τPhI(26)
232	4.81	1.11	-	-	τPhII(22), γCN(16), τCH3(11)
212	0.32	4.69	-	-	δPhI(31), δPhII(39)
188	3.78	1.68	-	-	τPhI(37), τCH_3(26)
183	1.13	1.24	-	190	δCN(40), τPhI(10), τPhII(10)
165	1.02	3.96	-	-	δCO(31), τPhII(23), δCN(15)
160	0.36	0.19	-	163	δCH_3(74), τCH_3(16)
115	0.66	1.3	-	-	τPhI(22), γCN(22), τPhII(10)
98	3.56	1.11	-	-	τC=O(54), τCH_3(17)
87	3.7	0.76	-	102	τCO(61), τCH_3(22)

75	2.38	0.85	-	-	γCN(31), δCN(23)
51	3.26	3.53	-	-	τCN(27), γCN(23), τPhI(10)
45	0.85	2.04	-	-	τCN(53), τPhI(13)
34	5.36	0.84	-	-	τCN(58)
16	2.86	1.1	-	-	γCN(56), τPhII(10), τC=O(10)

[a]υ-stretching; δ-in-plane deformation; γ-out-of-plane deformation; τ-torsion; PhI-phenyl ring; PhII-piperazine ring.

Table 6. Second-order perturbation theory analysis of Fock matrix in NBO basis corresponding to the intramolecular bonds of the title compound

Donor(i)	Type	ED/e	Acceptor(j)	Type	ED/e	E(2)[a]	E(j)-E(i)[b]	F(i,j)[c]
C2-C3	σ	1.984	N1-C7	σ*	0.029	2.480	1.080	0.046
-	-	-	N4-C16	σ*	0.084	2.360	1.100	0.046
N4-C16	σ	1.989	C3-N4	σ*	0.028	1.410	1.160	0.036
-	-	-	N4-C5	σ*	0.028	1.450	1.160	0.037
C5-C6	σ	1.983	N1-C7	σ*	0.029	2.720	1.070	0.048
-	-	-	N4-C16	σ*	0.084	1.930	1.090	0.042
C7-C8	σ	1.983	N1-C2	σ*	0.026	2.440	1.030	0.045
-	-	-	N1-C7	σ*	0.029	1.490	1.150	0.037
-	-	-	C7-C12	σ*	0.023	3.550	1.250	0.060
-	-	-	C8-C9	σ*	0.025	3.150	1.260	0.056
-	-	-	C9-O13	σ*	0.026	3.680	1.090	0.057
-	π	1.669	N1-C2	σ*	0.026	1.360	0.590	0.027
-	-	-	C7-C8	π*	0.425	1.360	0.280	0.018
-	-	-	C9-C10	π*	0.470	27.600	0.270	0.080
-	-	-	C11-C12	π*	0.308	12.790	0.290	0.055
C8-C9	σ	1.975	N1-C7	σ*	0.029	3.590	1.170	0.058
-	-	-	C7-C8	σ*	0.022	3.470	1.270	0.059
-	-	-	C9-C10	σ*	0.031	3.970	1.250	0.063
-	-	-	C10-N15	σ*	0.098	4.220	1.030	0.060
C9-C10	π	1.975	C7-C8	π*	0.425	13.940	0.280	0.056
-	-	-	C9-C10	π*	0.470	2.240	0.280	0.023
-	-	-	C11-C12	π*	0.308	25.160	0.300	0.079
-	-	-	N15-O37	π*	0.623	23.880	0.170	0.060
C10-N15	σ	1.989	C8-C9	σ*	0.025	1.540	1.350	0.041
-	-	-	C9-C10	σ*	0.031	1.540	1.350	0.041
-	-	-	C11-C12	σ*	0.014	1.700	1.400	0.044
N15-O37	π	1.986	C9-C10	π*	0.470	3.240	0.450	0.039
-	-	-	N15-O37	π*	0.623	7.100	0.340	0.052
C16-C18	σ	1.987	N4-C5	σ*	0.028	4.040	0.980	0.056
LPN1	σ	1.763	C2-C3	σ*	0.022	1.990	0.630	0.033
-	-	-	C5-C6	σ*	0.019	1.910	0.640	0.033
-	-	-	C7-C8	σ*	0.022	1.880	0.830	0.037
-	-	-	C7-C8	π*	0.425	32.390	0.290	0.090
LPN4	σ	1.696	C2-C3	σ*	0.022	4.030	0.610	0.048
-	-	-	C5-C6	σ*	0.019	3.890	0.620	0.047
-	-	-	C16-O17	π*	0.281	62.420	0.280	0.118
LPO13	σ	1.962	C8-C9	σ*	0.025	7.580	1.100	0.082

-	π	1.815	C9-C10	π*	0.470	35.280	0.330	0.104
LPO17	σ	1.976	N4-C16	σ*	0.084	1.970	1.130	0.043
-	-	-	C16-C18	σ*	0.055	1.930	1.050	0.040
-	π	1.864	N4-C16	σ*	0.084	26.340	0.700	0.123
-	-	-	C16-C18	σ*	0.055	20.040	0.620	0.101
LPO36	σ	1.981	C10-N15	σ*	0.098	4.210	1.090	0.062
-	-	-	N15-O37	σ*	0.060	2.410	1.220	0.049
-	π	1.898	C10-N15	σ*	0.098	12.580	0.580	0.076
-	-	-	N15-O37	σ*	0.060	18.440	0.710	0.103
-	-	-	N15-O37	π*	0.623	1.100	0.170	0.014
-	n	1.467	N15-O36	σ*	0.063	1.930	0.690	0.037
-	-	-	N15-O37	π*	0.623	148.770	0.150	0.137
LPO37	σ	1.981	C10-N15	σ*	0.098	4.280	1.080	0.062
-	-	-	N15-O36	σ*	0.063	2.620	1.200	0.051
-	π	1.898	C10-N15	σ*	0.098	13.510	0.580	0.079
-	-	-	N15-O36	σ*	0.063	19.690	0.700	0.106

[a]E(2) means energy of hyper-conjugative interactions (stabilization energy in kJ/mol)
[b]Energy difference (a.u) between donor and acceptor i and j NBO orbitals
[c]F(i,j) is the Fock matrix elements (a.u) between i and j NBO orbitals

Table 7. NBO results showing the formation of Lewis and non-Lewis orbitals

Bond(A-B)	ED/e[a]	EDA%	EDB%	NBO	s%	p%
σX2–X3	1.984	49.99	50.01	0.7070($sp^{2.61}$)C+	27.70	72.30
-	-0.634	-	-	0.7072($sp^{2.60}$)C	27.77	72.23
σN4–X16	1.989	63.88	36.12	0.7993($sp^{1.71}$)N+	36.89	63.08
-	-0.823	-	-	0.6010($sp^{2.18}$)C	31.36	68.64
σX5–X6	1.983	49.27	50.73	0.7019($sp^{2.61}$)C+	27.67	72.33
-	-0.627	-	-	0.7123($sp^{2.58}$)C	27.92	72.08
σX7–X8	1.971	50.47	49.53	0.7104($sp^{1.81}$)C+	35.54	64.46
-	-0.709	-	-	0.7038($sp^{1.83}$)C	35.38	64.62
πX7–X8	1.669	42.12	57.88	0.6490($sp^{99.99}$)C+	0.01	99.99
-	-0.265	-	-	0.7608($sp^{1.00}$)C	0.00	100.00
σX8–X9	1.975	49.97	50.03	0.7069($sp^{1.89}$)C+	34.63	65.37
-	-0.720	-	-	0.7073($sp^{1.62}$)C	38.22	61.78
πX9–X10	1.625	41.03	58.97	0.6405($sp^{1.00}$)C+	0.01	99.99
-	-0.269	-	-	0.7679($sp^{1.00}$)C	0.01	99.99
σX10–N15	1.989	38.23	61.77	0.6183($sp^{2.91}$)C+	25.56	74.44
-	-0.804	-	-	0.7860($sp^{1.76}$)N	36.20	63.80
πN15–O37	1.986	40.59	59.41	0.6371($sp^{99.99}$)N+	0.12	99.88
-	-0.438	-	-	0.7708($sp^{99.99}$)O	0.26	99.74
σX16–X18	1.987	48.68	51.32	0.6977($sp^{1.76}$)C+	36.26	63.74
-	-0.640	-	-	0.7164($sp^{2.76}$)C	26.56	73.44
n1N1	1.763	-	-	$sp^{15.22}$	6.16	93.84
-	-0.275					
n1N4	1.696	-	-	$sp^{99.99}$	0.51	99.49
-	-0.255					
n1O13	1.962	-	-	$sp^{1.68}$	37.33	62.67
	-0.544					
n2O13	1.815	-	-	$sp^{1.00}$	0.01	99.99
-	-0.319					
n1O17	1.976	-	-	$sp^{0.71}$	58.32	41.68
-	-0.669					
n2O17	1.864	-	-	$sp^{1.00}$	0.01	99.99
-	-0.240					

n1O36	1.981	-	-	$sp^{0.33}$	75.03	24.97
-	-0.777					
n2O36	1.898	-	-	$sp^{99.99}$	0.05	99.95
-	-0.269					
n3O36	1.467	-	-	$sp^{99.99}$	0.16	99.84
-	-0.254					
n1O37	1.981	-	-	$sp^{0.34}$	74.6	25.4
-	-0.774					
n2O37	1.898	-	-	$sp^{99.99}$	0.03	99.97
-	-0.267					

[a] ED/e is expressed in a.u.

Table 8: The docking results of the title compound with the human GABA receptor.

Binding Sites	HB score	SI score	Ligand conformation penalty	Total Score
A	-6.000	-53.167	6.611	-52.556
B	-5.513	-52.730	6.671	-51.572
C	-6.596	-59.781	7.910	-58.468
D	-8.628	-51.792	6.624	-53.795
E	-5.886	-53.699	6.687	-52.898

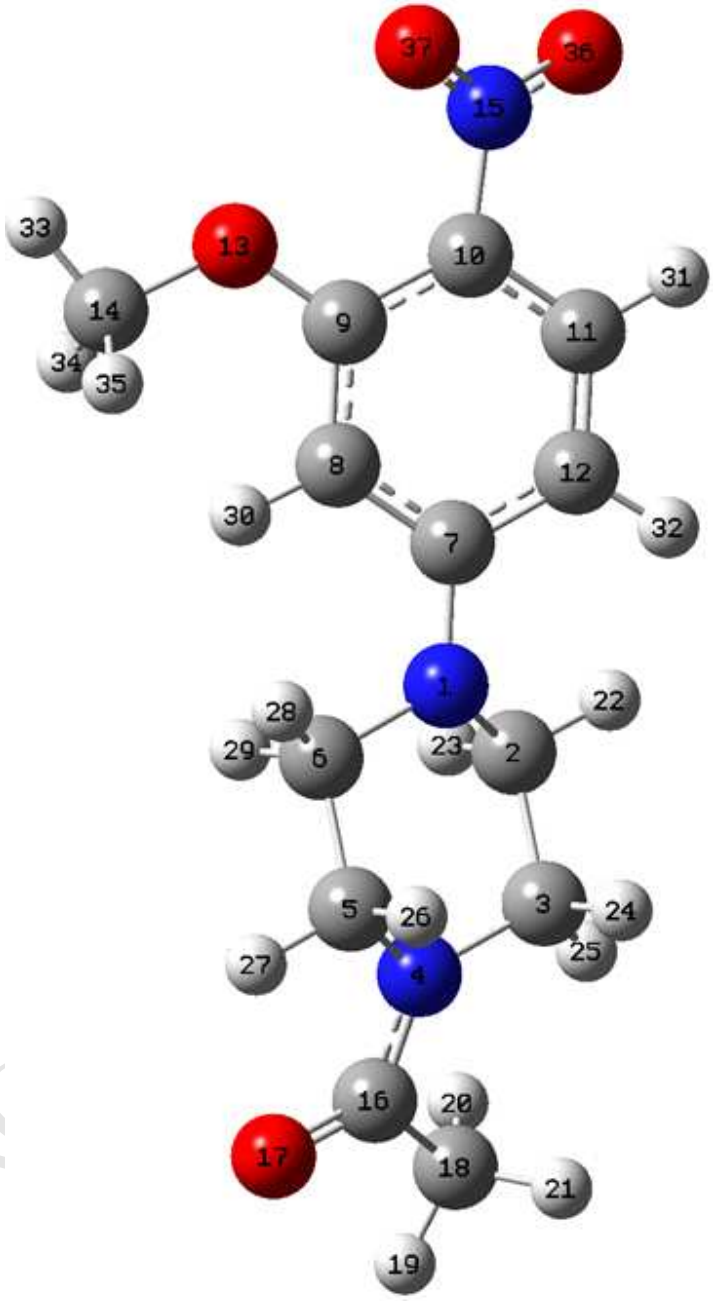

Figure 1. Molecular structure and atom numbering of MNPE.

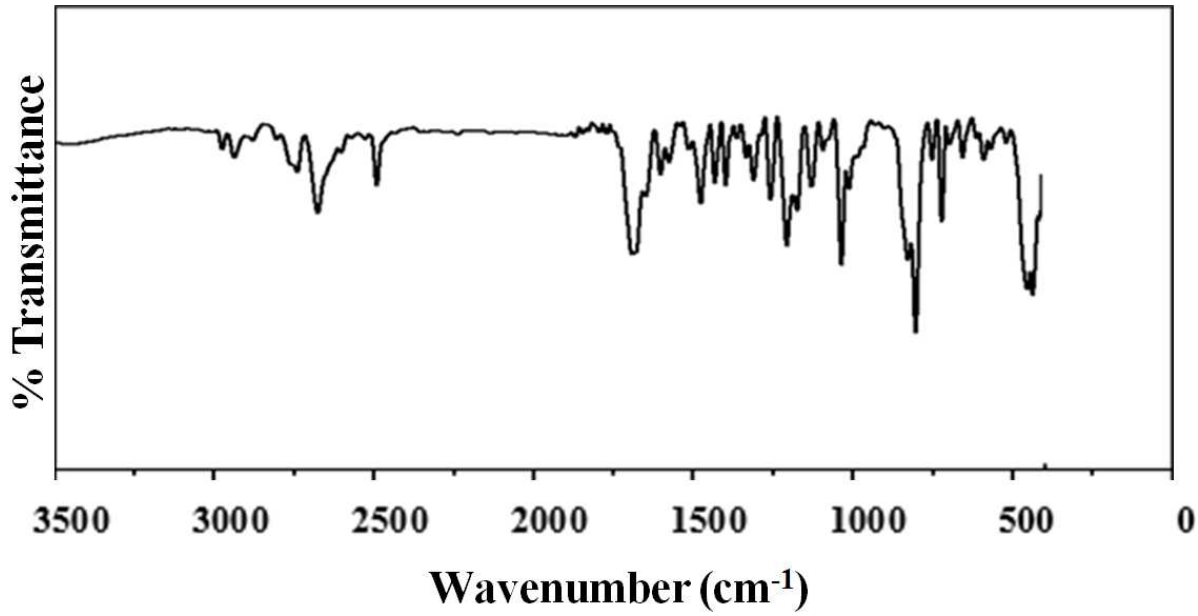

Figure 2. The mid-infrared spectrum of MNPE.

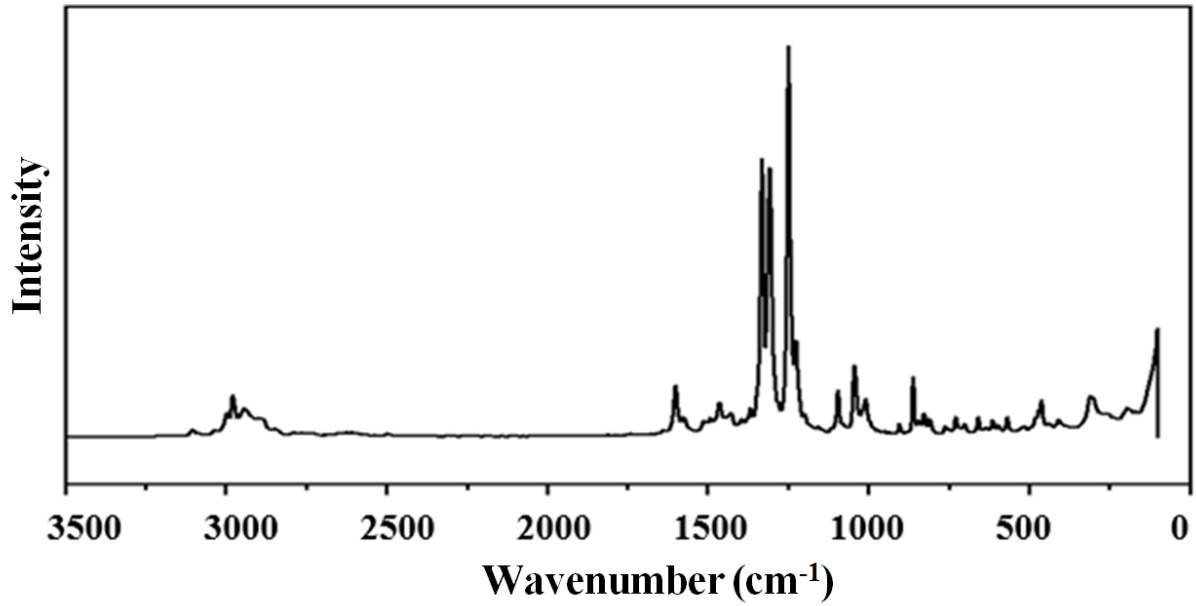

Figure 3. The Raman spectrum of MNPE.

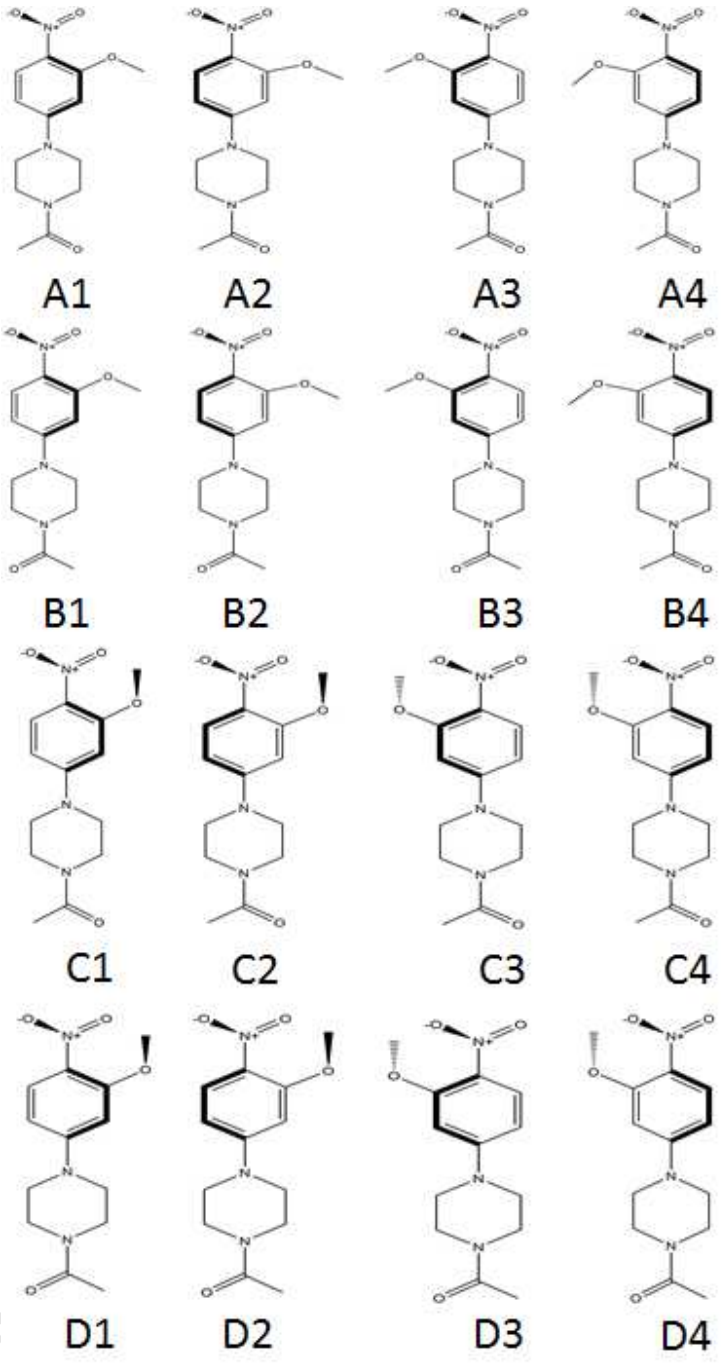

Figure 4. Calculated stable conformations of MNPE.

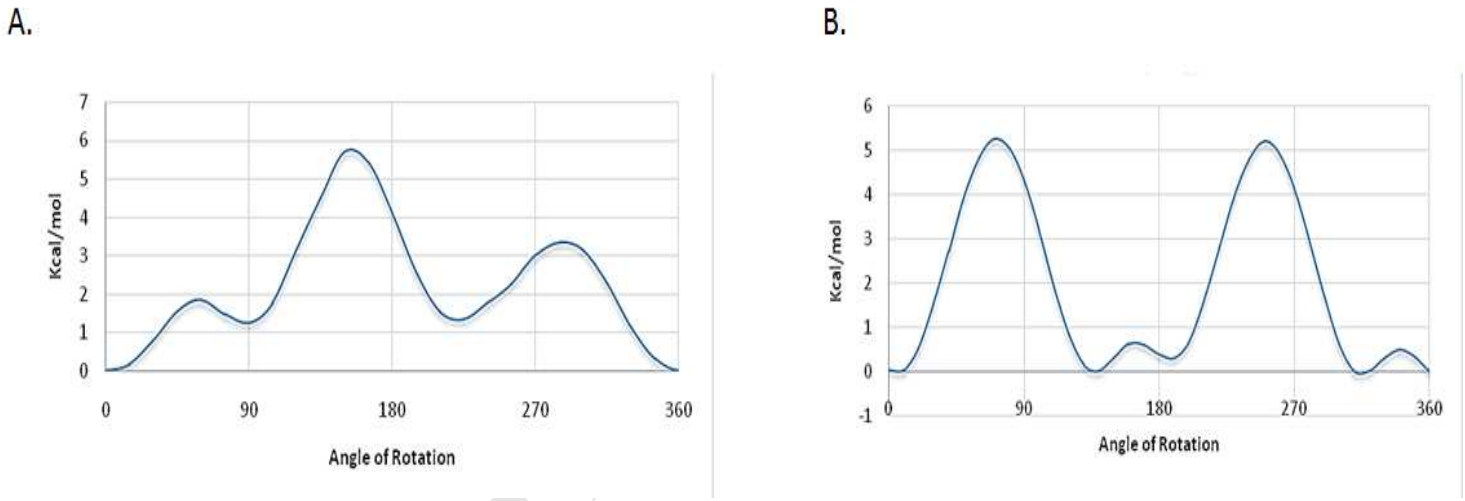

Figure 5. (A) Potential energy scan of C_8-C_9-O_{13}-C_{14} . (B) Potential energy scan of C_2-N_1-C_7-C_8 .

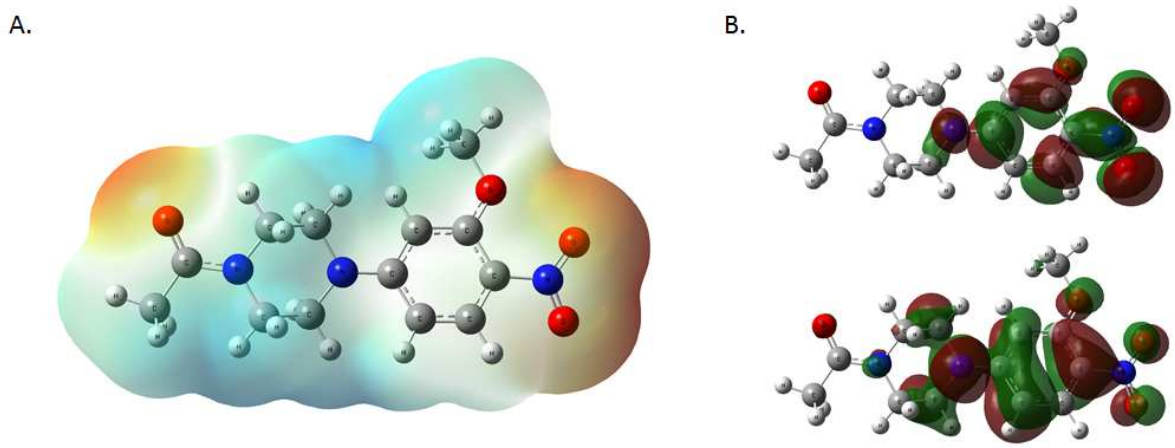

Figure 6. (A) Molecular Electrostatic Potential (MEP) map and (B) the LUMO (top) and HOMO (bottom) diagrams of MNPE.

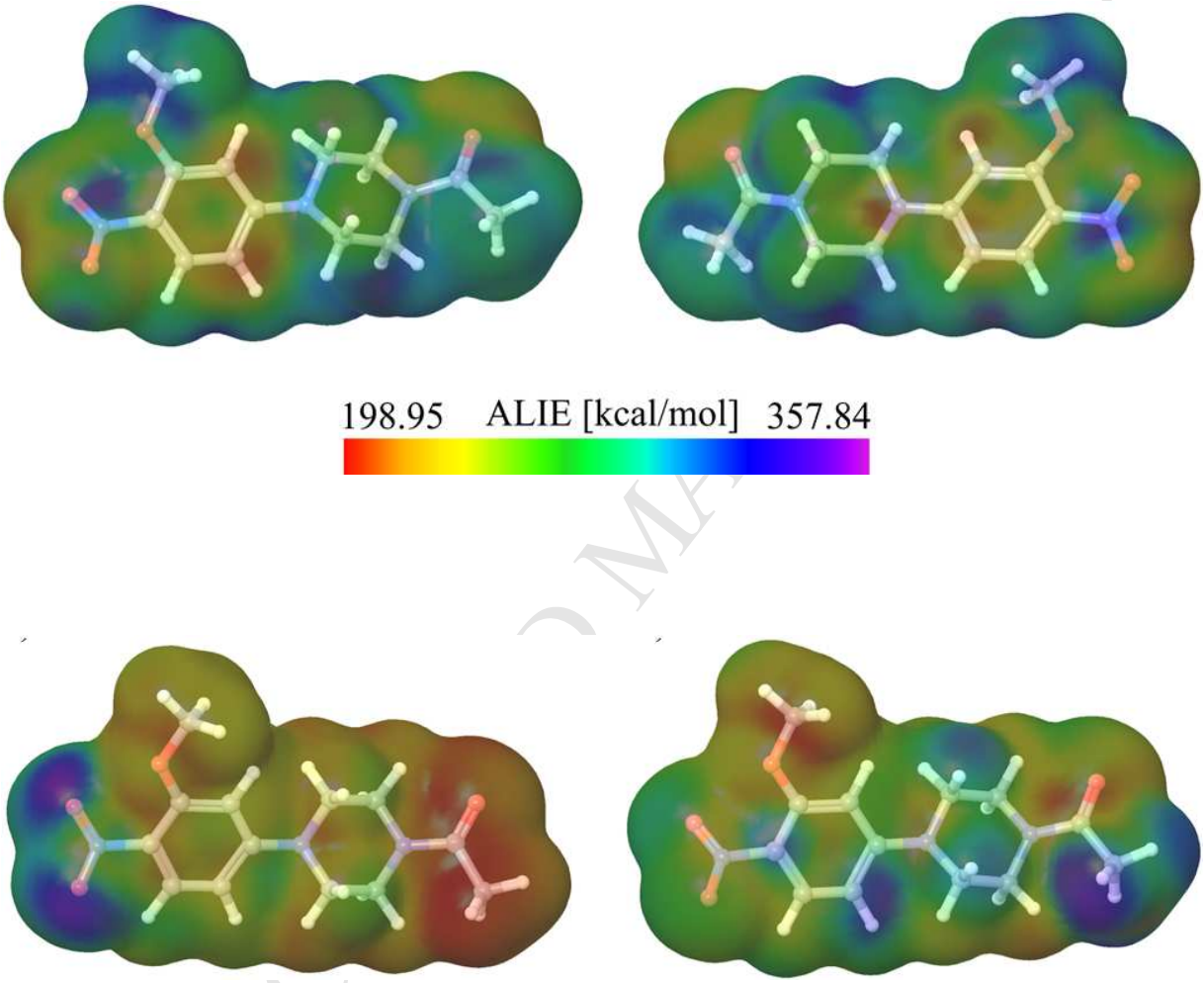

Figure 7. (A) Representations of the ALIE and (B) Fukui function surfaces of MNPE.

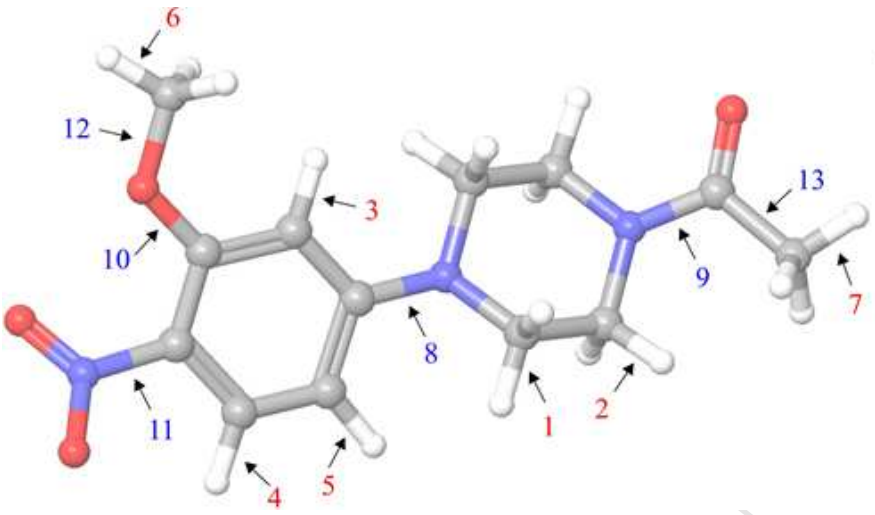

Bond	BDE [kcal/mol]
1	93.48
2	96.55
3	114.00
4	118.26
5	116.09
6	102.07
7	102.81
8	90.85
9	86.72
10	93.23
11	68.74
12	65.67
13	83.63

Figure 8. The BDE sites and values of MNPE. Values provided in red color are those for hydrogen abstraction, while blue color BDEs are for the rest of the single acyclic bonds

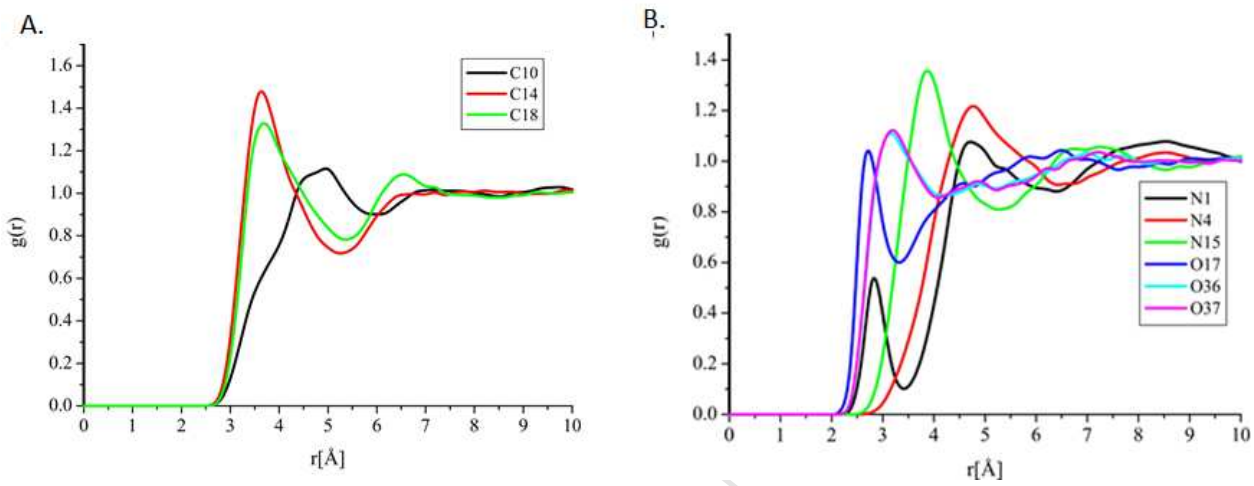

Figure 9. The plots showing the MNPE molecule areas that are prone to interactions with water molecules using RDF.

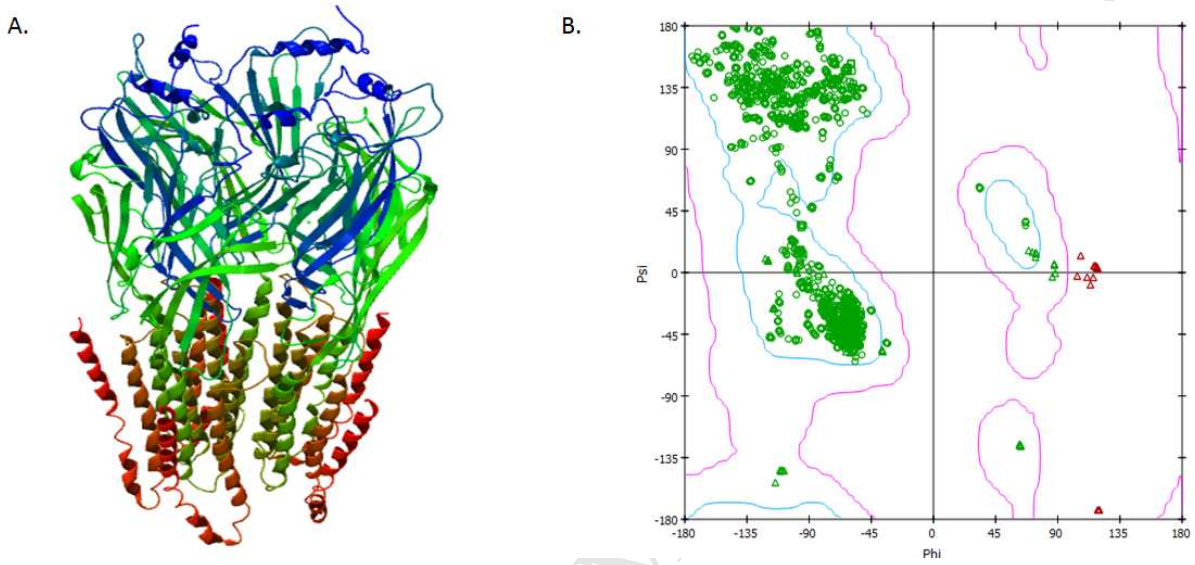

Figure 10. (A) The crystal structure of a human GABA receptor (PDB ID: 4COF). (B) The Ramachandran plot of the crystal structure of a human GABA receptor (PDB ID: 4COF).

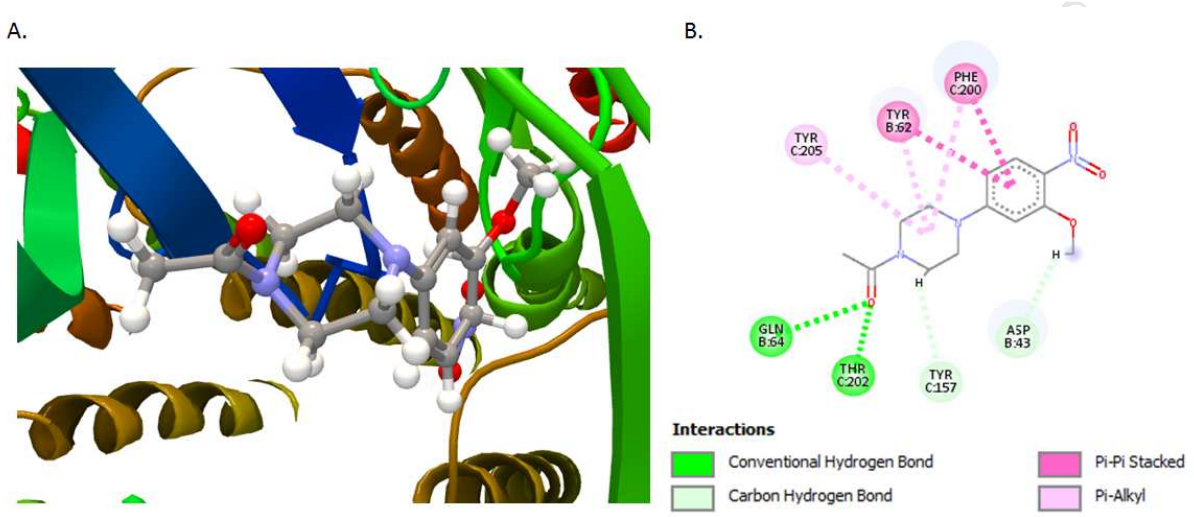

Figure 11. (A) Docked conformation of the title compound in binding site C of GABA (PDB ID: 4COF). (B) The molecular interactions of MNPE and amino acids in binding site *C* of GABA

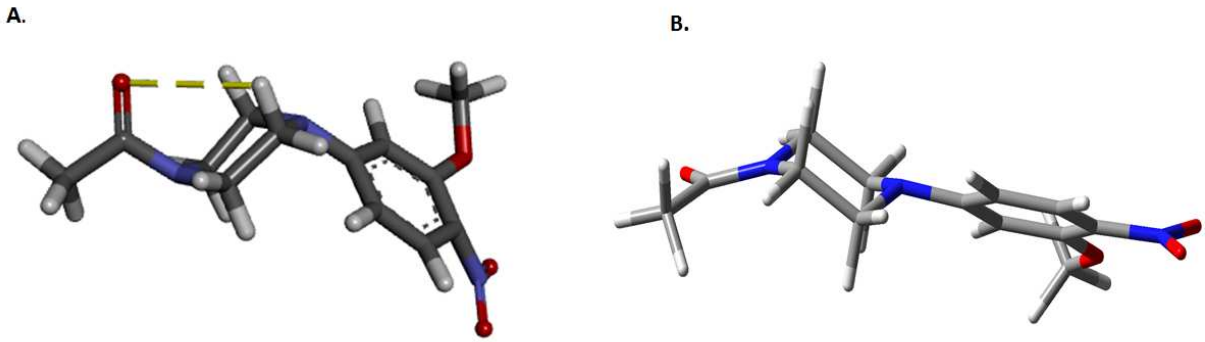

Figure 12. (A) Docked conformation of the title compound in binding site *C* showing the presence of intra-hydrogen bond (shown as yellow color). (B) The most stable conformation, B4 of the title compound

HIGHLIGHTS

- A new bioactive arylpiperazine-based drug has been synthesized and characterized.
- Complete vibrational spectroscopic assignments have been performed.
- Average Local Ionization Energies (ALIE) and Fukui functions were calculated.
- Molecular docking predicted a potential anti-stress activity for the newly synthesized compound.